Chapter 1

Heavy ion physics

In this chapter a quick overview of the physics of heavy ions is presented. After a general introduction, the study of dimuon production in heavy ion collisions is specifically addressed. The dilepton production from DY, charmed hadron decays, thermal sources, low mass and high mass resonance decays is described. The dimuon excess measured by the CERES, HELIOS/3 and NA38/NA50 experiments in previous analysis of the low and intermediate mass region are discussed and compared with some of the existing theoretical interpretations.

When the structure of the vacuum is violently
disturbed in a high energy nuclear collision
and the soft and colourless hadronic world
suffers the intrusion of the abundantly
produced coloured gluons and quarks..... (D.Kharzeev)

1.1 Introduction

Statistical Quantum Chromodynamics predicts that, in nuclear matter under high temperature and/or energy density conditions, a deconfined state of quark and gluon would be created, the quark gluon plasma (QGP). The temperature reached in the interaction volume of a heavy ion collision at SPS, where $\sqrt{s}$=17.22÷19.37, should be high enough to motivate the search for the predicted phase transition. Important indications on the nature of the mechanisms responsible for the confinement of quarks in hadrons and for the spontaneous chiral symmetry breaking could come from the study of the QGP. Furthermore, cosmological and astrophysical issues such as primordial black hole evaporation, cosmological nucleosynthesis and the search for a dark matter candidate could be better understood. Moreover, the core of neutron stars could consist of a low temperature and high density plasma of quarks and gluons, whose equation of state could be calculated if the equation of state of the high temperature-high density QGP formed in heavy ion collisions was known.

1.2 The phase transition

The strong interaction between partons inside hadrons is characterised by the so called asymptotic freedom at small distances and by a steep grow of the binding force as the distance between the constituents becomes larger, the so called colour confinement. This is due to the typical behaviour of the coupling constant α_s of strong interactions, which increases with growing distance between the constituent quarks. This is the reason why in ordinary nuclear matter quarks are confined inside hadrons.

At sufficiently high temperature and/or density (3 to 5 times higher than the ordinary nuclear matter density) a phenomenon similar to the Debye (charge) screening in a dense medium takes places. In a dense medium, the Coulomb potential between two electric charges, say a proton and a electron, is screened by the presence of a high density of negative charges surrounding the positive one, and it accordingly changes,

$$V(r) = \frac{e}{r} \rightarrow \frac{e}{r} \exp\left(-\frac{r}{r_d}\right) \tag{1.1}$$

where r_d is the Debye radius and $r_d \sim 1/\rho$ if ρ is the matter density. As r_d becomes smaller and smaller, the material undergoes the transition from insulator to (semi)conductor. For the same reason, the colour interquark potential

$$V(r) = \sigma r - \frac{\alpha}{r} \tag{1.2}$$

will experience screening in a medium characterised by a very high density of colour charges. The effect of the screening can be parametrised as

$$V(r,T) = \left(\frac{\sigma}{\mu(T)}\right)\{1 - e^{-\mu(T)r}\} - \frac{\alpha}{r}e^{-\mu(T)r} \tag{1.3}$$

were $\mu(T)$=$1/r_c$ is the screening mass and r_c is the colour screening radius : when r_c becomes very small, the potential goes to zero causing the hadrons to dissolve[1]. Quarks confined in a hadron have a non zero mass because of the interaction with the other quarks and gluons. When quarks become free in the deconfined phase, their masses drop to smaller values which ideally tend to zero. The bare or current-quark masses are $m_u \simeq 1.5 \div 5$ MeV, $m_d \simeq 3 \div 9$ MeV and $m_s \simeq 60 \div 170$ MeV[2]. The dropping of the quark masses would cause the so called chiral symmetry restoration of the QCD Lagrangian, where the latter is defined by

$$L_{QCD} = -\frac{1}{4}F^a_{\mu\nu}F^{\mu\nu}_a - \sum_f \overline{\psi}^f_\alpha(i\gamma^\mu\delta_\mu + m_f - g\gamma^\mu A_\mu)^{\alpha\beta}\psi^f_\beta \tag{1.4}$$

The so called chiral operator is the operator γ_5 which causes the chiral rotation of the quarks four-spinor, i.e.,

$$\psi \rightarrow \psi' = e^{(i\alpha\gamma_5)}\psi \tag{1.5}$$

The mass term $\overline{\psi}\psi$ in the QCD Lagrangian is not invariant under such rotation as

$$\overline{\psi'}\psi' = \overline{\psi}e^{(2i\alpha\gamma_5)}\psi \neq \overline{\psi}\psi \tag{1.6}$$

All the other terms in the Lagrangian are invariant under this operation because the matrices γ_μ anti-commute, by definition, with the matrix γ_5. It is quite clear then why a non zero quark mass destroys the chiral symmetry of the Lagrangian, from which the name of chiral symmetry restoration in the case of zero quark masses. In fact, interactions are never really turned off and only a partial chiral symmetry restoration is thus expected. Furthermore, it is still a matter of discussion if the chiral symmetry restoration coincides with the deconfinement or not.

Perturbative QCD can only be applied for small values of the QCD coupling costant. When studying nuclear matter under extreme density and/or temperature conditions, the perturbative approach has to be substituted by models or lattice QCD calculations[3][4]. Lattice QCD calculations predict that the phase transition should take place at the critical energy density ϵ=$2\div3$ GeV/fm^3 corresponding to $T_c \simeq 260$ MeV for a pure gluon plasma and $T_c \simeq 150$ MeV when 2 light quarks are included. It is therefore important to establish if such energy densities are actually released in the interaction volume of a heavy ion collision at SPS energies. This can be done measuring the transverse energy of the collision, defined as

$$E_T = \sum_i E_i \sin\theta_i \tag{1.7}$$

where the sum runs over all the secondary particles (mainly pions) produced in the interaction. In practice, the sum runs over the secondaries which can actually be detected. The transverse energy is usually measured by mean of a hadron calorimeter. In NA38/NA50 practical reasons suggested the use of an electro-magnetic calorimeter or EMCal. The NA50 EMCal measures the energy deposited in the calorimeter by the neutral pions produced in the collision. The relation between energy density and transverse energy is model dependent. Two very different descriptions are given by the fireball model, which calculates the energy density with the assumption of complete stopping in the collision, and the Bjorken model, which assumes a complete transparencies of the two colliding nuclei. The first model can be used when considering low energy heavy ion collisions as, for instance, in the Au-Au collisions at AGS; in this case the stopping power has been measured to be very large, i.e., most of the baryon content of the incoming nuclei can be found in the interaction region. Since in Pb-Pb collisions at the SPS energies only few tenth of nucleons can be found in the interaction volume, the NA38/NA50 Collaboration calculates the energy density from the measured transverse energy on the basis of the Bjorken model, i.e.

$$\epsilon = 3\frac{E_T^0}{\Delta y S_T \tau_0} \tag{1.8}$$

where τ_0 is the so called formation time, i.e. the time needed to pass from the initial hadronic to the partonic degrees of freedom, S_T is the transverse area interested by the collision and Δy is the covered rapidity interval. The factor 3 in eq.1.8 is needed to take into account the transverse energy of the charged secondaries.
The energy density profiles for very central 200 A GeV/c S-U and 158 A GeV/c Pb-Pb collisions are shown in fig.1.1. The average energy density is similar in the two cases, but in Pb-Pb collisions the locally deposited energy density can be 30-40% larger than in S-U collisions. The probability that a quark gluon plasma can be formed is therefore larger in very central Pb-Pb collisions than in very central S-U ones.

1.3 Experimental signals of the phase transition

Many theoretical models predict which kind of new physics would indicate the creation of a deconfined volume of matter in a heavy ion collisions. Strange matter enhancement, thermal dilepton and photon production, J/ψ suppression, charm thermal production are some of the predicted signals. Experimentally, the differential distributions of the dilepton produced in heavy ion collisions can be studied, as later explained. Dileptons can be produced in the semi-leptonic decay of the secondary hadrons in the collision or in the electro-magnetic annihilation of confined or deconfined partons.

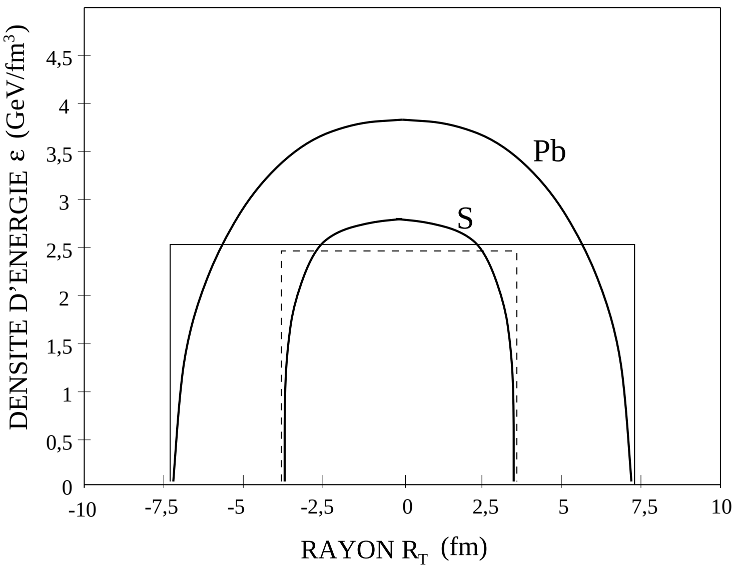

Figure 1.1: *Energy density profile calculated for central 158 A GeV/c Pb-Pb and 200 A GeV/c S-U collisions. The 'Rayon' R_T measures the transverse nuclear size.*

The present section describes important issues as J/ψ suppression, strangeness enhancement, thermal dimuon and charm production and vector meson $in - medium$ modification. In section 1.6 the DY and charm hadro-production processes, whose understanding is essential to the goal of the present thesis, are discussed in some more details. The last section is then dedicated to the discussion of the low and intermediate mass dilepton enhancement measured by NA38/NA50, CERES and HELIOS/3 at the CERN SPS.

1.3.1 Production and suppression of $c\overline{c}$ states

In 1986, Matsui and Satz[5] proposed the J/ψ suppression as an unambiguous signal of the formation of the quark gluon plasma. Since then, many improvements have been done in the understanding of the underlying physics. The 200 GeV/c p-A and 200 A GeV/c S-U NA38 data[6] can be well reproduced by the so called colour octet model. It this model, both the J/ψ and the ψ' are produced as a coloured $(c\overline{c})_8 g$ state. The coloured $(c\overline{c})_8 g$ state propagates in the surrounding medium and can therefore be broken by interactions with gluons which would couple either to the collinear gluon or to the coloured $(c\overline{c})_8$. This would suppress the J/ψ and ψ' production in exactly the same way, resulting in a constant $\psi'/J/\psi$ ratio. If the $(c\overline{c})_8 g$ state survives, the colourless resonance is created with the absorption of the collinear gluon by the $(c\overline{c})_8$ system.

Once the resonance has been formed, it can be suppressed through the exchange of hard gluons with the co-moving mesons produced in the collision,

$$\psi' + h \longrightarrow D + \overline{D} + X \tag{1.9}$$

Since the ψ' has a much lower binding energy than the J/ψ, 60 MeV and .64 GeV respectively, it can be easily broken in co-movers interactions. This theory well reproduces the $\frac{J/\psi}{DY}$ and $\frac{\psi'}{J/\psi}$ behaviour found in p-A and S-U collisions by the NA38 Collaboration. The measured $\frac{\psi'}{J/\psi}$ is constant for all p-A data but falls down in S-U collisions due to the ψ' suppression by final state interaction with the hadrons produced in the collision. The multiplicity of hadrons in the final state increases with the collision centrality and so does the ψ' suppression.
The NA50 Collaboration has reported a first evidence of strong J/ψ suppression in Pb-Pb collisions at 158 A GeV/c[7]. The observed suppression can not be explained in the frame of the above described theory. Models based on the comover absorption mechanism can not account for both the S-U and Pb-Pb results at the same time[6], whilst a successful reproduction of all data can be obtained in the hypothesis that a deconfined system has been created in central Pb-Pb collisions.

1.3.2 Strangeness enhancement

In 1982 J.Rafelski and B.Muller predicted that strangeness production would be enhanced in a QGP[8]. In a QGP, strange quarks would be abundantly produced in the processes :

$$q\overline{q} \longrightarrow s\overline{s} \tag{1.10}$$

$$gg \longrightarrow s\overline{s} \tag{1.11}$$

(where $q = (u, d)$), because of their dropping mass and because the Fermi levels for the lighter quark species would be quickly filled; the production of s quarks would then be favoured by the Pauli exclusion principle.
Experimentally, an enhancement in strangeness production could be seen as an enhanced strange meson and baryon yield, as ϕ, Λ, $\overline{\Lambda}$, Ω, Ξ, and/or via the appearance of strange matter lumps (the so called 'strangelets'[9]). At the CERN SPS three experiments have been mainly dedicated to this specific signature, WA85, WA94 and WA97[10]. WA85 and WA94 used the 200 A GeV/c S beam, whilst WA97 uses the 158 A GeV/c Pb one. The NA38/NA50 Collaboration has also measured the strangeness enhancement in d-A (A=C,U), 200 A GeV/c S-U and 158 A GeV/c Pb-Pb collisions[11]. Whilst the WA85, WA94 and WA97 experiments measure the production of multistrange hyperons, such as Λ, Ω and Ξ, the NA38/NA50 Collaboration measures the ratio $\phi/(\rho + \omega)$, assuming the ρ and the ω meson to remain unaffected by the hot and dense surrounding medium. The WA97 experiment recently observed a strangeness enhancement, with respect to extrapolation from p-Pb results, which increases with centrality and with the strangeness content of the hyperon[10].

1.3.3 Open-charm thermal production

In 1988-89, Shor[12, 13] studied the possibility of thermal charm production in a quark gluon plasma. His calculations, based on Bjorken hydrodinamical model, showed that the charm thermal contribution could eventually become important for temperature of the plasma above 500 MeV. Even if this was the case, only a slight open-charm enhancement in the dimuon mass spectrum below 1.5-2 GeV/c^2 would be seen.

In a recent publication[14], the charm thermal production in a quark gluon plasma has been studied for the future experiments RHIC and LHC where the energy density should be large enough to enable the QGP creation. The temperature T in the interaction volume is predicted to amount to $\simeq 0.35 \div 0.55$ GeV at RHIC ($\sqrt{s}$=200 A GeV) and to $\simeq 0.7 - 1$ GeV at LHC ($\sqrt{s}$=5.5 A TeV). In the proposed model, partons in a QGP would acquire temperature dependent effective masses favouring the creation of heavy quarks. The final thermal $c\bar{c}$ yield strongly depends on the adopted charm mass. At SPS the temperature in the interaction volume is just above the critical temperature predicted by lattice QCD calculations and the thermal charm production by massive gluons and quarks in a QGP seems highly improbable.

1.3.4 Thermal dileptons

Thermal dileptons can be produced either in a QGP or in a thermalized hadron gas[15, 16, 17]. Thermal dilepton production in a QGP is due to quark and antiquark annihilation in the thermalized medium. This process differs from the DY pair production process, which is due to a single-pair annihilation of hard quarks; thermal dimuons are produced after the quarks from the nucleons have thermalized through the exchange of a number of gluons with the surrounding partons[18]. Thermal dileptons generated in a dense thermalized hadron gas are produced in hadronic secondary collisions such as,

$$\pi\pi \longrightarrow l\bar{l} \tag{1.12}$$

$$\pi\rho \longrightarrow l\bar{l} \tag{1.13}$$

$$\pi a_1 \longrightarrow l\bar{l} \tag{1.14}$$

$$\pi\omega \longrightarrow l\bar{l} \tag{1.15}$$

$$K\overline{K} \longrightarrow l\bar{l} \tag{1.16}$$

$$K\overline{K}^* + c.c. \longrightarrow l\bar{l} \tag{1.17}$$

Both thermal dileptons from a QGP and/or from a dense hadron gas would give precious informations on the temperature of the volume of matter where they were generated.

In ref.[19] the contribution of dimuons generated in a *hadron gas* in the mass range $1< M <2.5\ GeV/c^2$ of the dilepton spectrum is carefully calculated. It is found that the dilepton yield from a hadron gas strongly depends on the temperature and that the most important contribution to the thermal dileptons is due to the $\pi a_1 \longrightarrow l\bar{l}$ annihilation process. This is shown in fig.1.2, where the predicted thermal yield from a hadron gas within the HELIOS/3 experimental acceptance is depicted for central S-W collisions.

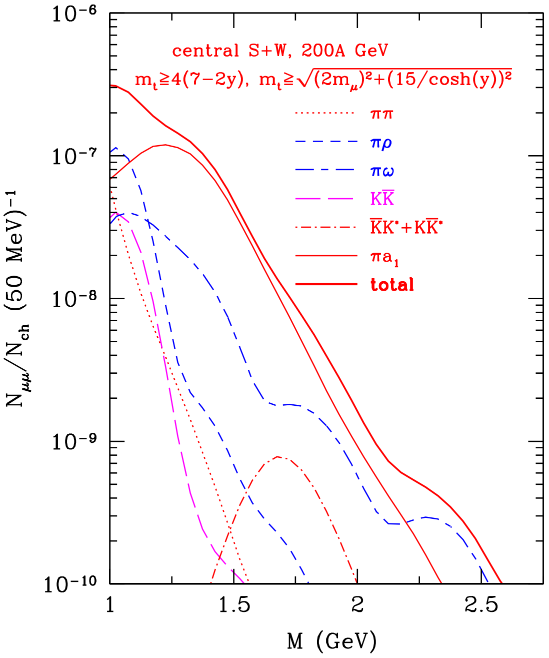

Figure 1.2: *Dimuon spectra in central S-W collisions at 200 A GeV/c from different secondary process as calculated in ref.[19].*

In ref.[20] the expected thermal dimuon contribution from the hot QGP phase and the subsequent HG has been calculated for SPS energies. Different equation of states, corresponding to different values of the critical temperature T_c, have been used. Different initial conditions (IS), corresponding to different initial energy densities and velocity profiles, have also been considered for each equation of state. The theoretically predicted thermal dimuon mass shape depends on the initial conditions for masses $\geq 2\ GeV/c^2$, as shown in fig.1.3. The mass spectrum shape in the IMR should be therefore used to distinguish between different inital state conditions. Since in the IMR M$\gg T_c$, where $T_c \approx$200 MeV, the main contribution comes from thermal dimuons produced in the hot initial phase.

In ref.[17], the different shapes of the contribution of dileptons from the hadron gas and from the QGP phase to the measurable dilepton mass spectra is depicted for AGS energies. The contribution from the $\pi\pi$ annihilation channel, which dominates from the $2m_\pi$ threshold up to 1 GeV/c^2, is predicted to be suppressed if a QGP is created. This is due to the larger hadronic density in the hadronic scenario, where hadrons are produced in the first stages of the system evolution. For M> 2 GeV/c^2 the contribution of dilepton from the elementary $q\overline{q}$ annihilation in the QGP is predicted to be larger than the contribution from the $\pi\pi$ annihilation channel.

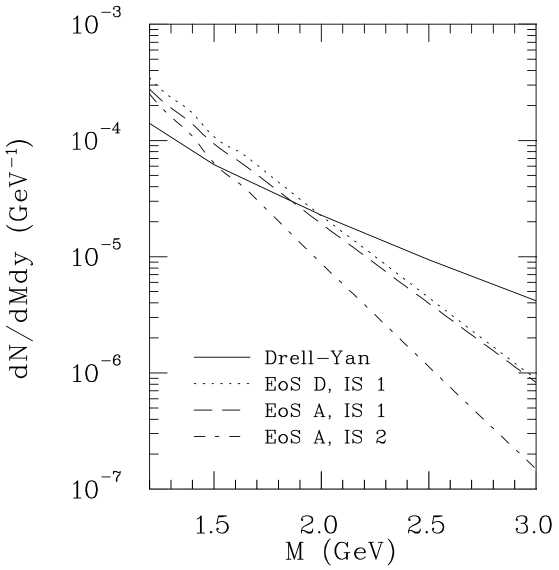

Figure 1.3: *Calculated mass distribution of thermal electron pairs compared to the calculated distribution for DY dileptons at* $y_{CM} = 0$. *No kinematic cuts have been applied[20].*

The comparison of the above theories with experimental results is later discussed.

1.3.5 Vector meson in-medium characteristics

If chiral symmetry is restored in the hot and dense volume of matter created in heavy ion collisions, the vector meson masses should drop to lower values. Dilepton pairs are generated through vector meson decay

$$V \longrightarrow l^+ l^- \tag{1.18}$$

The study of vector mesons is complicated by the fact that leptons are generated at different times in the interaction volume history. This makes it difficult to deconvolute the signals and separate leptons coming from regions of different temperature and/or baryonic density.

Because of its very small life time, Γ =150.7$\pm$1.1 MeV, the ρ meson can decay inside the interaction volume, when its actual mass is still affected by the state of the lump of matter created in the collision. There exist many different models trying to predict the mass and width evolution of vector mesons and of the ρ meson in particular, and not all of them agree in predicting a lowering of its mass with increasing temperature and/or baryonic density[21, 22]. In the following section some of the most successful theoretical predictions and/or descriptions of experimental data are discussed.

1.4 Useful variables

I here give a brief definition of some important variables which will be widely used in the following of the present work.

In the collision of two hadrons, the hadron-hadron center-of-mass energy squared is defined as,

$$s = (p_1 + p_2)^2 \tag{1.19}$$

where p is the hadron four-momentum. In the collision, one parton from one of the two hadrons interacts with a parton from the other hadron. Each of the two interacting partons carries a fraction x of the four-momentum of the hadron it belongs to. For the system of the two colliding partons, the elementary parton-parton center-of-mass energy squared can be defined as

$$\hat{s} = x_1 x_2 s \tag{1.20}$$

where x_i is the *longitudinal momentum fraction* carried by the parton i.

The invariant mass of the elementary reaction is

$$M^2 = (x_1 p_1 + x_2 p_2)^2 \simeq x_1 x_2 s \tag{1.21}$$

A very widely used variable is the *rapidity* y

$$y = \frac{1}{2} ln \frac{(E + p_z)}{(E - p_z)} \tag{1.22}$$

When $p \gg m$ the rapidity y is well approximated by the *pseudo-rapidity* η

$$\eta = -ln(tan(\frac{\theta}{2})) \tag{1.23}$$

where θ is the particle polar angle. An important property of the rapidity y is the invariance of the shape of the rapidity distribution dN/dy with respect to a boost in the z-direction. This means that under a boost in the z-direction with velocity β, $y \rightarrow y + tanh^{-1}\beta$. If p_L^* is the longitudinal momentum and y^* the rapidity in the parton centre of mass frame, the following equation holds,

$$p_L^* = m_T \cdot \sinh y^* \tag{1.24}$$

From the above definitions, the *scaling* variable τ can be defined:

$$\tau \equiv \frac{M^2}{s} = x_1 x_2 \tag{1.25}$$

with which

$$x_1 = \sqrt{\tau} e^{+y^*} \tag{1.26}$$

$$x_2 = \sqrt{\tau} e^{-y^*} \tag{1.27}$$

The *longitudinal momentum fraction of the parton pair*, or Feynman variable x_F, is defined as

$$x_F \equiv \frac{2p_L^*}{\sqrt{s}} = x_1 - x_2 \tag{1.28}$$

1.5 The $Drell - Yan$ process

The Drell-Yan process consists of the electro-magnetic annihilation of a (valence or sea) quark and an antiquark of the same flavour in a hadron-hadron interaction, as shown in fig.1.4. In the annihilation, a lepton pair is created along with some unobserved hadrons.

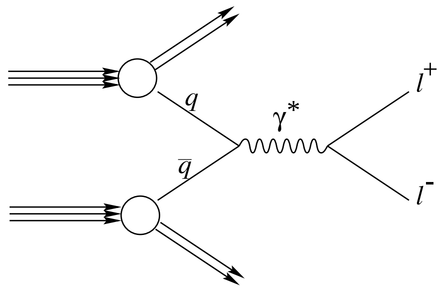

Figure 1.4: *The DY process.*

The cross-section for the elementary process

$$q_i\overline{q_i} \to \gamma^* \to l^+l^- \tag{1.29}$$

is

$$\frac{d\sigma}{d\Omega}\mid_{c.m.s.}= \frac{4\alpha^2}{16M^2}e_i^2(1+cos^2\theta) \tag{1.30}$$

which integrated gives

$$\sigma_i(q_i\overline{q_i} \to \gamma^*) = \frac{4\pi\alpha^2}{3M^2}e_i^2 \tag{1.31}$$

where e_i is the quark electric charge and M is the invariant mass of the produced l^+l^- pair. If we take into account the probability of finding the quark and the antiquark i in the hadrons A and B, we obtain for the DY differential cross section calculated in the frame of the naif parton model :

$$\frac{d^2\sigma}{dx_1dx_2} = \frac{1}{3}\frac{4\pi\alpha^2}{3M^2}\sum_i e_i^2[f_i^A(x_1)\overline{f_i^B}(x_2) + \overline{f_i^A}(x_1)f_i^B(x_2)] \tag{1.32}$$

where the $f_i^H(x_j)$, with H=A, B and $j = 1, 2$, are the so called *parton distribution functions* (PDF's). $f_i^H(x_j)dx$ represents the probability of finding the parton of type i in the hadron H, carrying a longitudinal momentum fraction between x_j and $x_j + dx$ of the total longitudinal hadron momentum. The factor 1/3 ensures that only parton-antiparton annihilation between partons of the same flavour are taken into account. When corrections to the cross-section 1.32 are added in the leading order approximation (LLA), eq.1.32 becomes

$$\frac{d^2\sigma}{dx_1dx_2} = \frac{4\pi\alpha^2}{9M^2}\sum_i e_i^2[f_i^A(x_1,Q^2)\overline{f_i^B}(x_2,Q^2) + \overline{f_i^A}(x_1,Q^2)f_i^B(x_2,Q^2)] \tag{1.33}$$

Q^2 is the so called *scale* where $Q^2 = -q^2$ if q^2 is the transferred four-momentum. The scale dependence in the DY cross section 1.33 is due to the inclusion of the leading corrections to the basic process in the so called leading log or leading order (LO) approximation. These corrections, mainly due to gluons, behave as $log(Q^2)$ and introduce singularities which are then re-absorbed redefining the PDF's. The absorption of the singularities through the redefinition of the PDF's is the *factorisation theorem.* The redefined PDF's depend on the scale Q^2 and their Q^2 evolution can be calculated with the GLAP (Grigov-Lipatov-Altarelli-Parisi) equations.

An important consequence of the *factorisation theorem* is the *universality* of the redefined PDF's. This means that the PDF's are the same for all pQCD processes.

In order to extract information on the PDF's, the cross sections for deep inelastic scattering (DIS) processes can be measured; from the measured cross sections, the nucleon structure functions can be deduced and the PDF's extracted. These PDF's can then be used in the calculation of the cross sections of different pQCD processes.

The LLA theoretical cross section underestimates the experimentally measured values by a factor ≈ 2. The ratio

$$K^{DY} = \frac{\text{experimentally measured cross section}}{\text{Theoretical prediction}} \tag{1.34}$$

measures the discrepancy between the theoretically computed and experimentally measured cross sections. In fig.1.5[7], the K^{DY}_{MRS-A} factor measured by NA38, NA51 and NA50 in p-p, p-d, p-A, S-U and Pb-Pb collisions is shown vs. $A \cdot B$, where A and B are the projectile and target atomic numbers. The measured K_{DY} does not show any energy dependence.

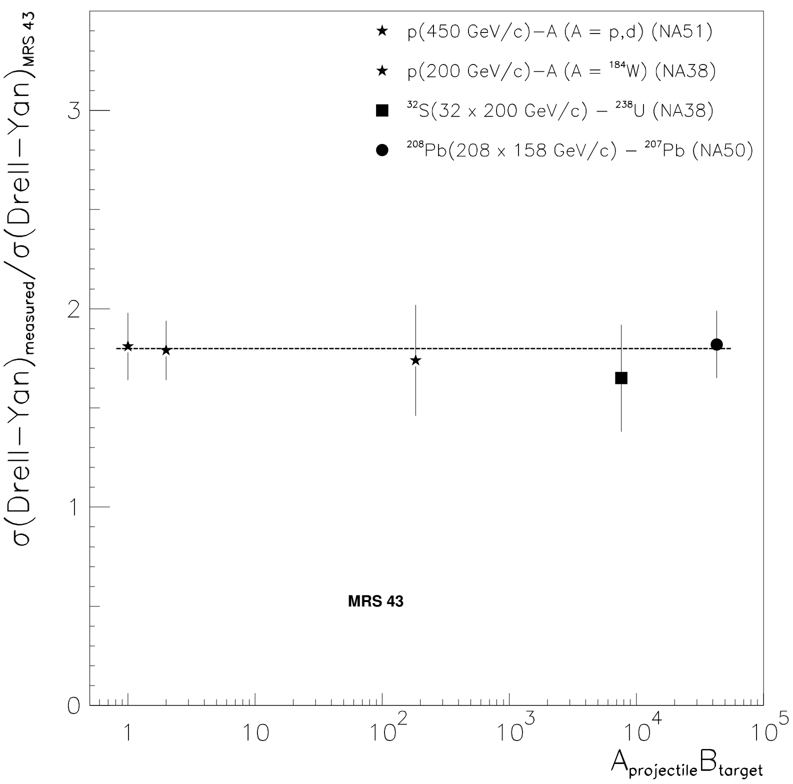

Figure 1.5: *The K^{DY} factor as measured by the NA38/NA51/NA50 experiments. The MRS A (set no.43) PDF's set has been used.*

The DY cross section depends on the valence quark contents of the two colliding hadrons. Therefore, the DY cross section in pp, pn, np, nn collisions is different.

The DY mechanism is a hard process and it is therefore expected to be insensitive to the state of the matter created in the collision. In this hypothesis, the DY nucleus-nucleus cross sections can be obtained as a weighted sum of all the pp, pn, np and nn elementary collisions. For instance, in the collision of two nuclei of atomic number A_1 and A_2, the DY cross section can be written as

$$\sigma_{AB}^{DY} = (Z_1 Z_2)\sigma_{pp} + [Z_1(A_2 - Z_2)]\sigma_{pn} + [Z_2(A_1 - Z_1)]\sigma_{np} + [(A_2 - Z_2)(A_1 - Z_1)]\sigma_{nn} \tag{1.35}$$

If σ_{NN} is the averaged DY cross section in nucleon-nucleon collisions, eq.1.35 can be written as

$$\sigma_{AB}^{DY} = \sigma_{NN}^{DY} A^{\alpha} B^{\alpha} \text{ with } \alpha = 1.0 \tag{1.36}$$

The value of α for the DY process has been experimentally measured in pA and AB collisions and confirms this simple picture. This is shown in fig.1.6 and, indirectly, in fig.1.5, where the measured and calculated DY cross sections are compared. Since the theoretical cross section is computed as from eq.1.35, the constant ratio plotted in fig.1.5 is equivalent to state that

$$K_{DY} \mid_{NN} = \frac{\sigma_{AB}^{DY} \mid_{meas.}}{\sigma_{NN}^{DY} \mid_{th} AB} = K_{DY} \mid_{AB} \tag{1.37}$$

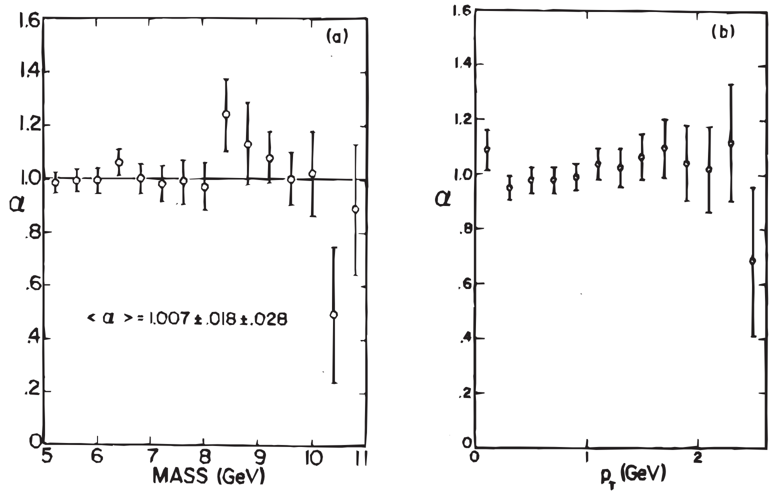

Figure 1.6: *The DY α value as a function of the invariant mass and the transverse momentum p_T as measured by the E288 experiment in 200 GeV/c proton induced collisions[23].*

Whilst the valence quarks in a hadron carry a substantial longitudinal momentum fraction x of the hadron momentum, the sea quark distributions are peaked at low

x values. Therefore, since the DY production in proton-nucleus or nucleus-nucleus collisions relies on the sea contents of the target nucleon, the cross section for DY production is small at large invariant mass M=$x_1 x_2$. Furthermore, since at very low mass DY pairs are mainly produced in sea-sea quark interactions, the isospin dependence of the DY cross section should decrease with the invariant mass of the produced lepton pair.
Many different sets of theoretical parton distribution functions exist as deduced from muon or neutrino deep inelastic scattering or related hard scattering data for different values of the transferred momentum Q^2. Modern parametrisations include the new results on the sea quark asymmetry, as measured by NA51[24]. In the frame of the naif parton model, the parton distribution functions of the light sea quarks $\overline{u}$ and $\overline{d}$ are supposed to be identical, i.e., the light quark sea is supposed to be symmetric, with $\overline{u}/\overline{d}$=1. In this hypothesis, the DY asymmetry, defined by

$$A_{DY} = \frac{\sigma_{pp} - \sigma_{pn}}{\sigma_{pp} + \sigma_{pn}} \tag{1.38}$$

is expected to be equal to 0.09 when the ratio $\lambda_V = u_V/d_V$ (V=valence) in a proton is equal to 2[24]. The DY asymmetry measured by NA51 clearly indicates that the symmetry of the light quark sea is broken. The measured value, A_{DY}=-0.09±0.02±0.025, corresponds to a sea quark ratio $\overline{u}/\overline{d}\simeq$0.51 for $\sqrt{\tau} = M/\sqrt{s} = 0.18$.

Up until when the new MRS A set[25, 26] including the light sea quark asymmetry as measured by NA51 was proposed[24], the NA38/NA50 Collaboration always adopted the GRV LO (1992)[27] set of nucleon structure functions [28]. In fig.1.7 the Drell-Yan asymmetry measured by NA51 and predicted by the old MRS H and CTEQ2M parametrizations and by the new MRS A is shown as a function of $\sqrt{\tau} = M/\sqrt{s}$. The MRS A PDF's are calculated at the next-to-leading order (NLO), which amounts to the inclusion of $O(\alpha_s)$ higher order corrections. Since at low Q^2 the perturbative approach ceases to be valid, the PDF's can be evolved down to $Q^2 \approx 4GeV^2$. For lower Q^2, the PDF evolution can be computed with ad-hoc effective parametrizations tuned to give a good reproduction of the experimental data, as in ref.[26]. The minimum allowed Q^2 in the MRS A (1995) set is $Q^2_{min,MRSA}$=0.625 GeV^2. The GRV LO (1992) set of functions also allows for very low Q^2, $Q^2_{min,GRVLO}$=0.250 GeV^2, but a different technique is used to deduce the low Q^2 behaviour of the PDF's[26].

PDF's in a nucleus and in a free nucleon

In fig.1.8[29], the ratio of the PDF's for gluons and for valence and sea quarks in a lead nucleus and in a free proton is plotted as a function of the longitudinal momentum fraction x carried by the partons. The shown curves, corresponding to two different values of the Q^2 scale, clearly indicate that the PDF's in a nucleus and

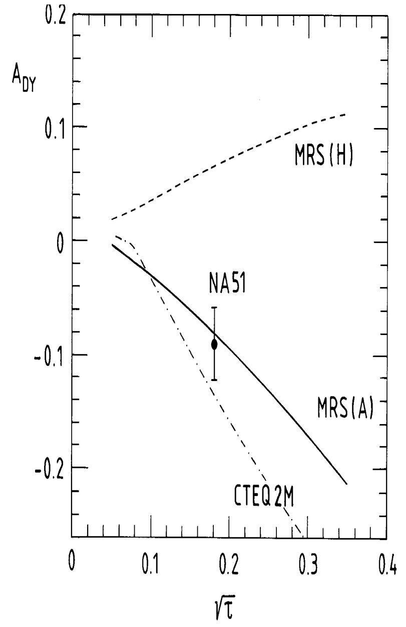

Figure 1.7: *The DY asymmetry in pp and pn collisions as a function of* $\sqrt{\tau} = M/\sqrt{s}$*. The MRS A set includes the results from the NA51 asymmetry measurement, whilst the MRS H and CTEQ2M are previous to it[25].*

in a free nucleon can strongly differ. The behaviour of R for gluon and quark with the Bjorken x can be subdivided in the following four different regions :

- The behaviour of R in the region below the value of x for which R=1, is denominated as shadowing; the gluon or quark component seen in a nucleus at small x is smaller than the one seen in a free nucleon. This effect is negligible in the NA38/NA50 acceptance window, where $x \geq 0.1$.

- When (and if) R becomes larger than 1, the corresponding effect is called anti-shadowing. In this case, the gluon or quark component seen in a nucleus at the corresponding x is larger than the one seen in a free nucleon. This effect is not negligible in the NA38/NA50 acceptance window as far as the gluon and valence quark component are concerned; since the DY process in nucleon-nucleon collisions mostly involves sea quarks, for which the effect is negligible, the anti-shadowing effect on the DY can be neglected.

- Then R starts decreasing again and reaches a minimum; the corresponding effect is named after the collaboration where it was originally measured (EMC)[30].

- The last rise of the ratio R is associated with the Fermi motion of nucleons within the nucleus; only when very large x (x >0.5) are investigated, the effect of Fermi motion has to be taken into account[31]. In the NA38/NA50 acceptance window this effect has been estimated to be negligible[32].

Eq.1.35 amounts to state that the modification of the PDF's in a nucleus with respect to the PDF's in a free nucleon do not play a substantial role as far as the DY cross section is concerned. On the other hand, in ref.[33] the DY α value is predicted to change as a consequence of the above modifications. In fig.1.9 the α dependence on the lepton pair invariant mass and collision energy is shown as calculated in ref.[33] in proton-gold collisions for $\sqrt{s} \geq 39$ GeV and for different PDF's. Even if the calculation has not been performed for 158 A GeV/c Pb-Pb collisions, from an extrapolation of the shown curves down to SPS energies we can argue that $\alpha \approx 1.0$, in agreement with experimental results.

The isospin correction

Since the DY cross section in proton-proton and proton-neutron collisions is not the same, a correction is needed when comparing the DY cross sections measured on systems characterised by a different protons to neutrons ratio. The so called isospin correction has to be applied on the measured cross sections, and amounts to calculate the DY cross section which would have been measured if the projectile and target nucleus were made by protons only.

For instance, if the DY cross section has been measured in A-B collisions, with A≥1 and B>1, the isospin correction can be calculated as

$$I_{DY} = \frac{\sigma_{pp}^{DY} \mid_{th.} \cdot A \times B}{\sigma_{AB}^{DY} \mid_{th.}} \tag{1.39}$$

where the two cross sections in eq.1.39 have to be derived using the same set of parton distribution functions. The isospin correction is then applied on the experimentally measured cross section, i.e.

$$\sigma_{AB}^{DY} \mid_{meas.}^{cor.} = \sigma_{AB}^{DY} \mid_{meas.} \cdot I_{DY} \tag{1.40}$$

which gives

$$\sigma_{AB}^{DY} \mid_{meas.}^{cor.} = K_{DY} \mid_{meas.} \cdot \sigma_{pp}^{DY} \mid_{th.} \cdot A \times B \tag{1.41}$$

The isospin correction has to be applied every time a comparison is drawn between DY cross sections or between ratios of cross sections where the DY is used as a reference.

1.6 Open-charm hadro-production

Hadrons consisting of charmed *and* non-charmed valence quarks are generically indicated as *open-charm*,

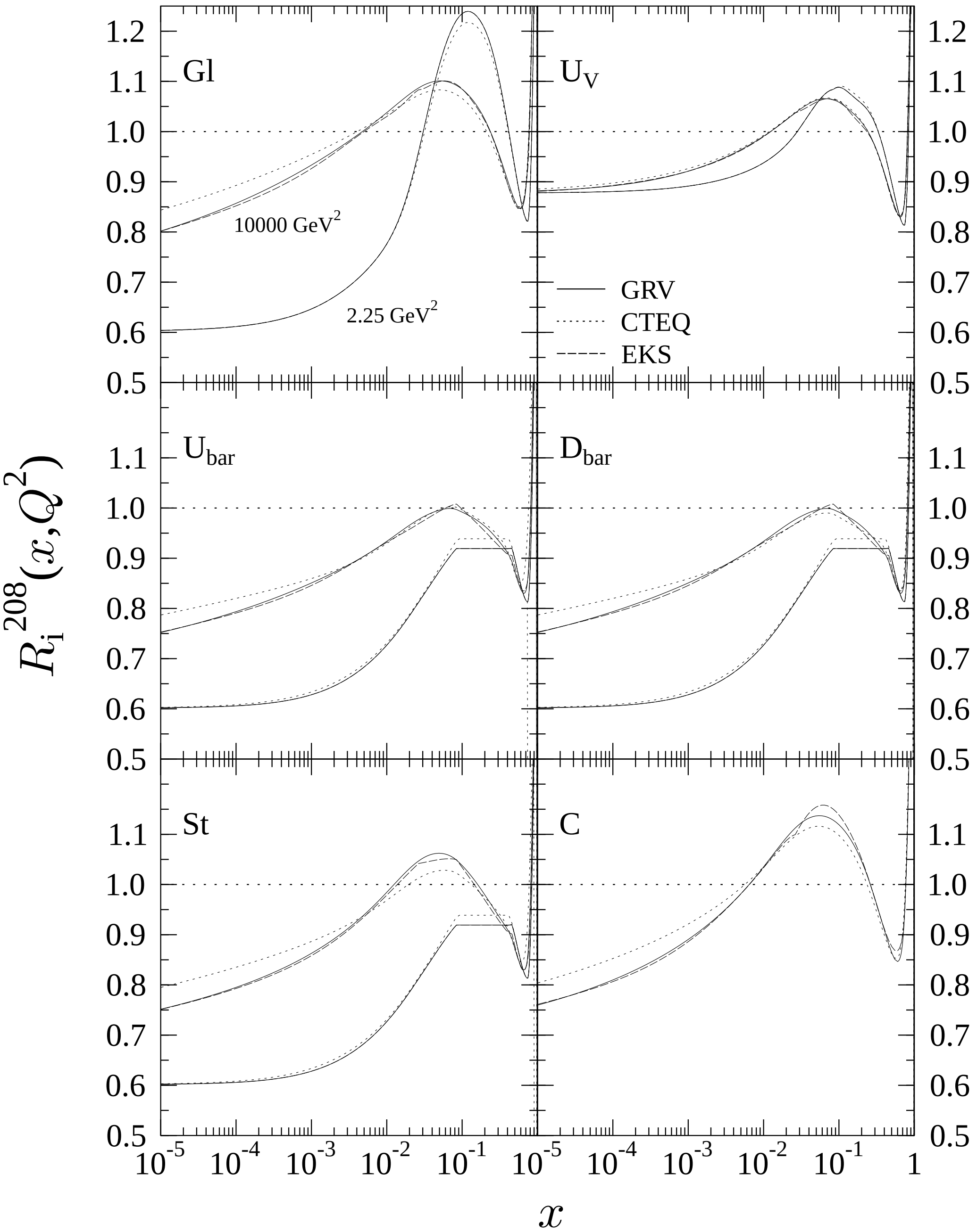

Figure 1.8: *The nuclear ratio $R^{A=208}$, defined as the ratio of the parton PDF in a lead nucleus and in a free proton, is plotted for the parton flavours i=g,u_V,$\overline{u}$,$\overline{d}$, s,c as a function of x and for two fixed values of Q^2=2.25 GeV^2 and Q^2=10000 GeV^2[29]. The two PDF's set GRV LO (solid lines) and CTEQ (dotted lines) have been used in the calculation of the free proton PDF's. The parametrization of the nuclear effect obtained with the GRV LO PDF's is also shown (ESK) as proposed by the authors in the same ref.[29].*

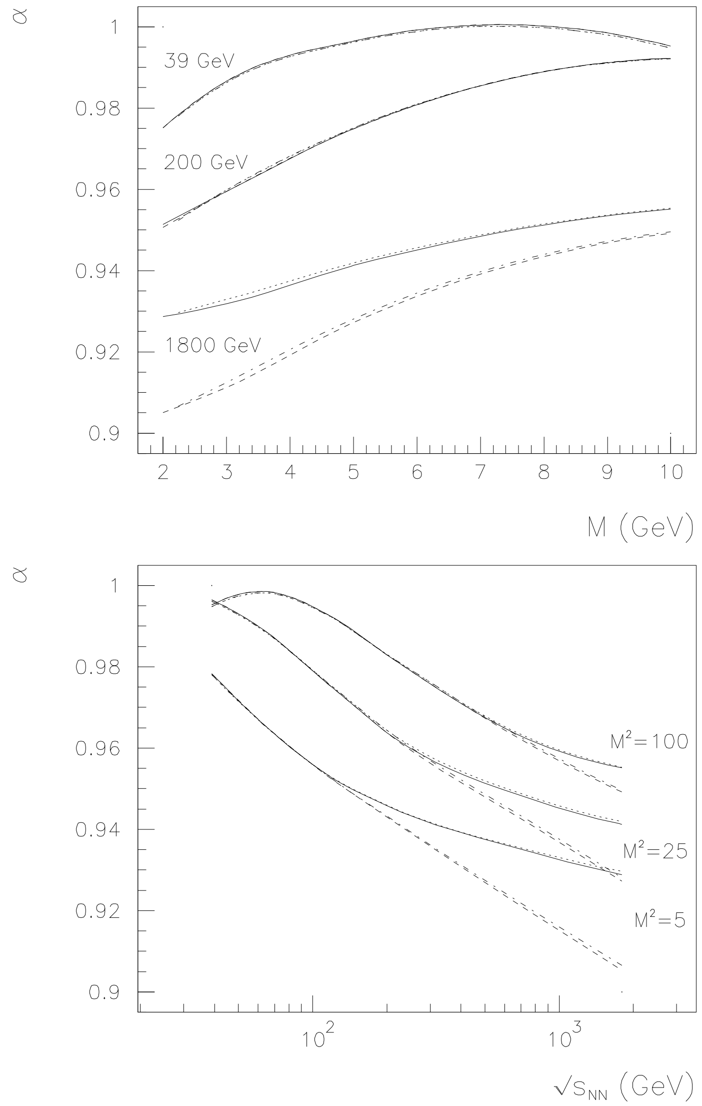

Figure 1.9: *Mass (top) and energy (bottom) dependence of α for DY pair production in proton-gold collisions for GRV HO (solid and dashed curves) and MRS-A (dotted and dashed-dotted curves)[33].*

- Charmed mesons (C= ± 1) :

$$D^+ \equiv (c\overline{d}) \text{ [M=1869.3±0.5 MeV]} \tag{1.42}$$

$$D^- \equiv (d\overline{c}) \text{ [M=1869.3±0.5 MeV]} \tag{1.43}$$

$$D^0 \equiv (c\overline{u}) \text{ [M=1864.6±0.5 MeV]} \tag{1.44}$$

$$\overline{D^0} \equiv (u\overline{c}) \text{ [M=1864.6±0.5 MeV]} \tag{1.45}$$

- Charmed-strange mesons (C = S = ± 1) :

$$D_s^+ \equiv (c\overline{s}) \text{ [M=1968.5±0.6 MeV]} \tag{1.46}$$

$$D_s^- \equiv (s\overline{c}) \text{ [M=1968.5±0.6 MeV]} \tag{1.47}$$

- Charmed baryons (C = +1) :

$$\Lambda_c^+ \equiv (udc) \text{ [M=2284.9±0.6 MeV]} \tag{1.48}$$

$$\Xi_c^+, \Xi_c^0 \equiv (qsc) \text{ [M=2465.6±1.4, 2470.3±1.8 MeV]} \tag{1.49}$$

$$\Sigma_c^+, \Sigma_c^0, \Sigma_c^{++} \equiv (q_1 q_2 c) \text{ [M=2453.6±0.9, 2452.2±0.6, 2452.8±0.6 MeV]} \tag{1.50}$$

$$\Omega_c^0 \equiv (ssc) \text{ [M=2704±4 MeV]} \tag{1.51}$$

Of all the semi-leptonic and hadronic decay modes, only the ones having one μ in the final state, e.g.

$$D \longrightarrow \mu\nu_\mu X \tag{1.52}$$

can contribute to the dimuon mass spectrum.

Open-charm hadro-production is described by leading order perturbative QCD as being mainly due to the process of 'fusion' of two partons,

$$gg \longrightarrow c\overline{c} \tag{1.53}$$

$$q\overline{q} \longrightarrow c\overline{c} \tag{1.54}$$

Since in the parton fusion model 80% of the produced open-charm originates from gluon fusion, no isospin correction is needed when comparing open-charm cross sections measured for different colliding systems.

The parton fusion model describes the open-charm hadro-production process as a superposition of elementary processes at the partonic level. In general, the cross section for the inclusive process $hh \rightarrow HX$, where h,H and X are hadrons, can be written as

$$d\sigma^{h_1 h_2 \rightarrow HX} = \sum_{a,b,c,d} \int dx_a dx_b dz \cdot f_1(x_a, Q^2) f_2(x_b, Q^2) \cdot d\sigma^{ab\rightarrow cd} D_H^d(z, Q^2) \tag{1.55}$$

where $d\sigma^{ab\rightarrow cd}$ is the cross section for the elementary process (a, b, c, d are generic partons) and $z = P_H/p_d$ is the fraction of the momentum of the hadronizing parton carried away by the hadron H. $D_H^d(z, Q^2)$ is the so called *fragmentation function* describing the fragmentation (hadronization) of the parton d in the hadron H. The Q^2 dependence of the fragmentation function originates from the factorisation theorem (see previous section) and fragmentation functions are considered to be *universal*. Fragmentation functions are calculated in the frame of phenomenologic models and then compared with the experimental cross section for the process $e^+e^- \rightarrow HX$, because the cross section for this process can be simply written as

$$d\sigma^{e^+e^-\rightarrow HX} = \sum_d d\sigma^{e^+e^-\rightarrow d\overline{d}} \cdot D_H^d(z, Q^2) \tag{1.56}$$

The *universality* of the fragmentation functions implies that the fragmentation process of the parton d in the hadron H is supposed to be completely independent from the projectile flavour composition.

The above described parton fusion model gives satisfactory results for x_F<0.5. The absolute value of the open-charm cross section has to be multiplied by a K factor, as for the DY process, to reproduce the measured cross section. The measured $K_{open-charm}$ is a function of the charm mass value used in the theoretical calculations and can also depend on the adopted PDF set. In this same model, the nuclear dependence of the open-charm hadro-production cross section can be simply parametrized as

$$\sigma_{pA}^{D\overline{D}} = \sigma_{pp}^{D\overline{D}} A^{\alpha} \tag{1.57}$$

with $\alpha = 1$. On the other hand, in ref.[33] α is predicted to depend both on the collision energy and on x_F. Fig.1.10 shows the calculated energy dependence for proton-gold interactions.

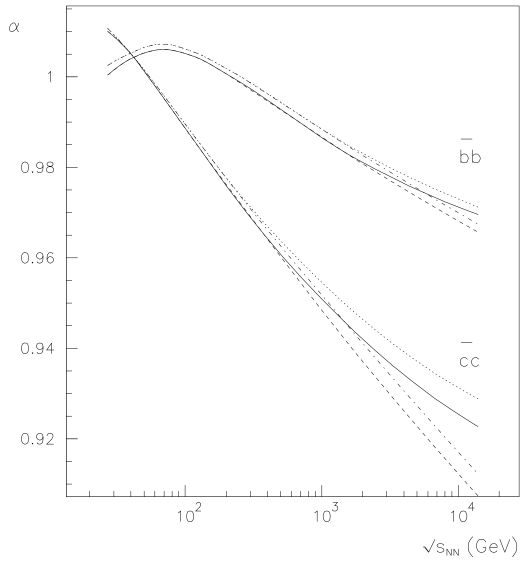

Figure 1.10: *Energy dependence of α for charm and beauty production in proton-gold collisions for GRV HO (solid and dashed lines) and MRS-A (dotted and dashed-dotted lines) PDF's[33].*

Furthermore, the parton fusion model alone does not fully reproduce the differential open-charm hadro-production cross sections $d^2\sigma/dx_F dp_T^2$ for x_F >0.5. Moreover, there is experimental evidence of an existing asymmetry in the cross section of leading and non-leading D meson production

$$A(x_F) = \frac{\sigma_{leading} - \sigma_{non-leading}}{\sigma_{leading} + \sigma_{non-leading}} \tag{1.58}$$

A charmed meson is said to be *leading* if it contains projectile valence quarks and *non-leading* if it does not; as an example, in $\pi^- \equiv (d\overline{u})$ induced reactions the D^0 and D^- are leading, whilst the $\overline{D^0}$ and the D^+ are not. The measured asymmetry implies that the fragmentation process depends on the quark content of the projectile.

Different models have been developed to explain the above mentioned non perturbative aspects of heavy quark hadro-production; in the following some of them are briefly described and their prediction compared with experimental results.

In the intrinsic-k_T model[34], intrinsic transverse momenta k_T are assigned to the incoming partons and then added to the total transverse momentum of the created heavy quark pair. If the fragmentation process is taken into account, for $\langle k_T^2 \rangle$=1.00 GeV^2/c^2 and m_c=1.5 GeV/c^2, a fair reproduction of experimental data can be obtained, as shown in fig.1.11. A better agreement can be achieved when the (too high) value $\langle k_T^2 \rangle$=2.00 GeV^2/c^2 is used for the same charm mass value or when $\langle k_T^2 \rangle$=1.00 GeV^2/c^2 but m_c=1.8 GeV/c^2. On the other hand this latter value for the charm mass is excluded when comparing pQCD NLO theoretical predictions with the $c\bar{c}$ total cross section measurement[34], as shown in fig.1.15 and later explained.

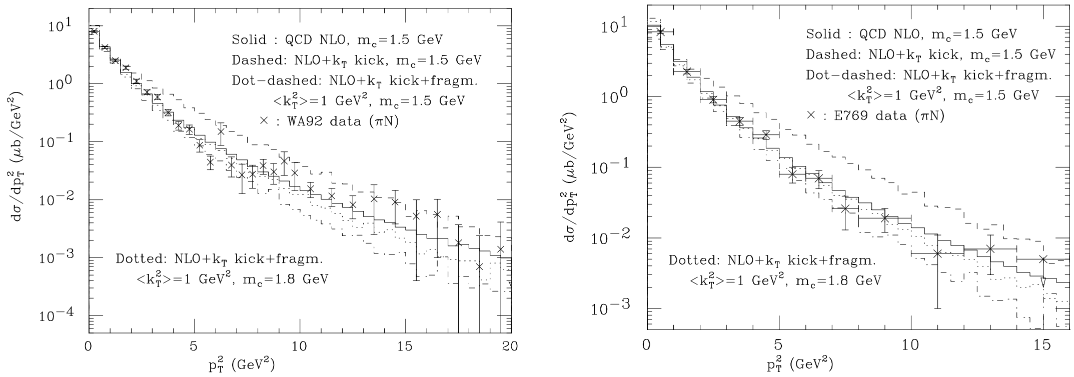

Figure 1.11: *Comparison between the single inclusive p_T^2 distributions measured in 350 GeV/c π^--N collisions by WA92 (left) and 250 GeV/c π^--N collisions by E769 (right) and the Next to Leading Order QCD predictions, with and without the inclusion of non-perturbative effects.*

The Intrinsic Charm Coalescence model[35, 36, 37] predicts the existence of the leading/non-leading asymmetry and tries to reproduce the differential cross section for open-charm production for x_F >0.5. It is based on the pQCD prediction that, at a certain order of the perturbative calculation, fluctuations of the projectile wave function could appear which would create virtual $q\bar{q}$ states within the projectile wave function itself. In proton induced reactions, where the parton composition of the projectile is (uud), the proton wave function at a certain time t could be thus described by ($uudc\bar{c}$). Soft interactions of the light valence quarks with the target can put the virtual $c\bar{c}$ on its mass-shell. Both charmed quarks can then either hadronize or independently coalesce with the co-moving valence quarks in the proton. When the c quarks hadronize, non-leading charmed hadrons are created, whilst leading charmed hadrons are generated through the coalescence mechanism. The intrinsically created charmed quarks co-move with the projectile valence quarks and therefore have large longitudinal momentum fraction x and a small p_T. Therefore, the effect of intrinsic coalescence could be seen at large longitudinal momentum x_F >0.5 and low p_T. The coalescence of the c quarks created via the intrinsic charm production process is an *initial* state process. Furthermore, the c quarks generated in the parton fusion process can also coalesce with collinear valence quarks. This *final* state coalescence can take place only when the $c\bar{c}$ pair has been created a very low p_T, where collinear quarks can be found. It is therefore expected to dominate when the created c quark and the valence quarks have the same velocity, at very

large x_F.
In the frame of the IC model, the cross section for open-charm production in pA collisions can be written as

$$\sigma^{pA} = \sigma^{pp}_{pf} A^{\alpha} + \sigma^{pp}_{ic} A^{\beta} \qquad (1.59)$$

where $\alpha \simeq 1$ and $\beta \simeq 2/3$ because the intrinsic process is a surface effect. If the predictions of the IC model were correct, the measured α should show a clear dependence on x_F. The α values measured in beam dump experiments[38], where the charmed hadrons were detected through the produced leptons (neutrino, muon) and no determination of the decay vertex was feasible, give an average value of $\langle\alpha\rangle$=0.79±0.03. The latter is larger than the predicted 2/3 when the above surface correction is taken into account, and lower than 1.0. In ref.[38] this, and the measured α dependence on x_F and the found leading meson asymmetry, are motivated by the existence of more than one production mechanism at the quark level, as predicted by the IC model. However, modern direct measurements of heavy quark production, with experimental apparatus allowing for a precise determination of the decay vertex, indicate that α is compatible with 1 and does not depend on x_F or p_T, as briefly summerized in the following.

In ref.[39] the nuclear dependence of charm hadro production has been measured with a 800 GeV/c proton beam on beryllium and gold targets, giving α=1.02±0.03±0.02. There is no evidence for any α dependence on either x_F or p_T, but this could be due to the limited range in x_F and p_T covered by the experiment, 0.0< x_F <0.08 and 0.0< p_T < 1.1 GeV/c.
The E769 experiment[40] has measured α=1.00±0.05±0.02 in 250 GeV/c π induced reactions on Be, Al, Cu and W targets. The E769 experiment covers the range $0 < p_T < 4$ GeV/c and $0 < x_F < 0.5$. They do not find any dependence of the measured α on the beam polarity (π^+ or π^-), transverse p_T or longitudinal x_F momentum of the detected D mesons or the type (neutral or charged) of D meson.
The WA92 experiment[41] has measured the charmed meson production in 350 GeV/c π^- induced reactions on Cu and W targets and in a wide x_F and p_T range : 0.0< x_F <0.8 and 0.0< p_T <7 GeV/c. They have also measured the leading meson asymmetry, finding an evident evolution of the asymmetry with x_F. No x_F or p_T dependence of α has been measured, as shown in fig.1.12. The found α=0.95±0.06±0.03 is in agreement with the parton fusion model predictions.

In order to check if the available data on open-charm hadro-production can be reasonably well described by leading order QCD calculations, in ref.[42] the prediction of the well known PYTHIA event generator have been compared with recent experimental measurement of differential and absolute open-charm cross sections. In fig.1.13 the $D\overline{D}$ x_F, p_T^2, mass and rapidity difference distributions from π-Cu collisions at $\sqrt{s}$=26 GeV/c[42] are also compared with the scaled PYTHIA predictions. Fig.1.14[42] shows the x_F and p_T distributions for D mesons produced in pp

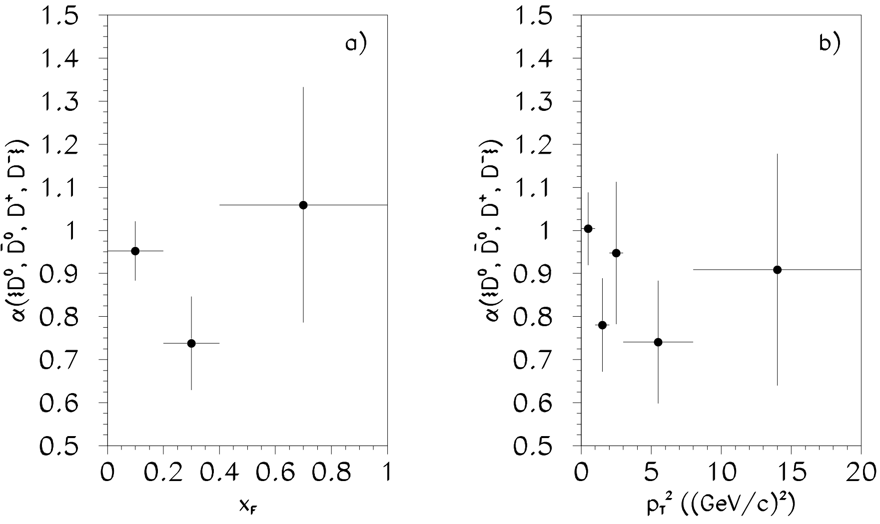

Figure 1.12: *Dependence of* $\alpha(\{D^0, \overline{D^0}, D^+, D^-\})$ *on* x_F *(left) and* p_T^2 *(right) as measured by the WA92 experiment[41].*

collisions at 250 GeV/c, compared with the leading order pQCD predictions of the PYTHIA event generator. In PYTHIA the dimuon transverse momentum originates from the intrinsic transverse momentum k_T assigned to the partons inside the colliding hadrons. PYTHIA reproduces reasonably well the experimental distributions if scaled up by an ad-hoc K-factor, leaving the shape of the PYTHIA distributions unchanged.

This is the reason why, as explained in chapter 4 and chapter 7 of the present thesis, the PYTHIA event generator has been used in the present work to generate the open-charm differential and absolute cross sections. Besides, in the NA38/NA50 acceptance window, x_F is never larger than ≈ 0.4, and dimuon from open charm are detected for $x_F \approx 0.2$; therefore, the above detailed higher twist effects can be comfortably neglected. On the other hand, when studying the open charm production in nucleus-nucleus collisions at SPS energies, since $x_1 \approx 0.2$ where the gluon anti-shadowing effect is large (see fig.1.8), the latter can increase the open charm dimuon produced in the NA38/NA50 acceptance window. This effect has been estimated to account for no more than 20% of the dimuon excess measured in nucleus-nucleus collisions at SPS (see chapter 7 and references therein).

The charm mass

The exact value of the charm mass is not precisely known. In fig.1.15, the cross-sections for charm (top part) and bottom (bottom part) pair production measured by FNAL and CERN experiments are shown[34]. The experimental points are compared with theoretical predictions based on QCD NLO calculations, using the MRS

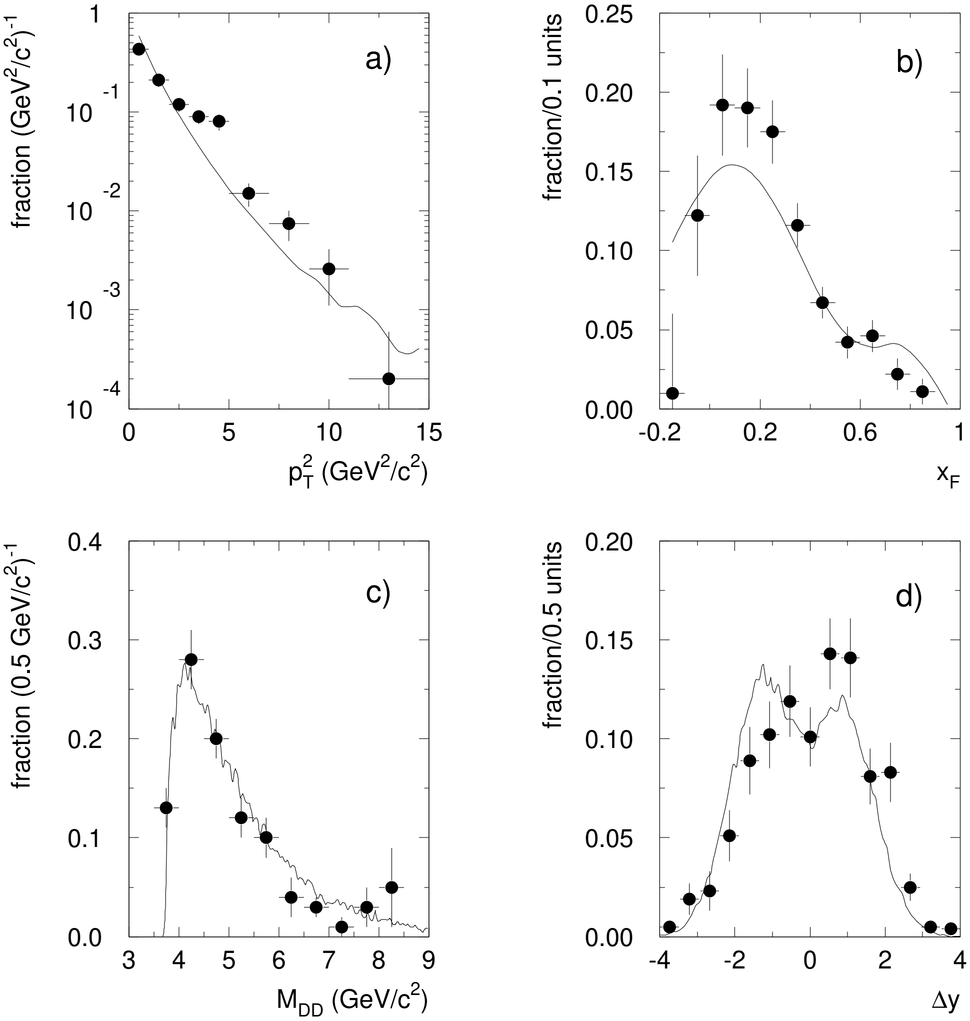

Figure 1.13: *$D\overline{D}$ x_F, p_T^2, mass and rapidity difference distributions from π-Cu collisions at $\sqrt{s}$=26 GeV/c compared with PYTHIA predictions[42].*

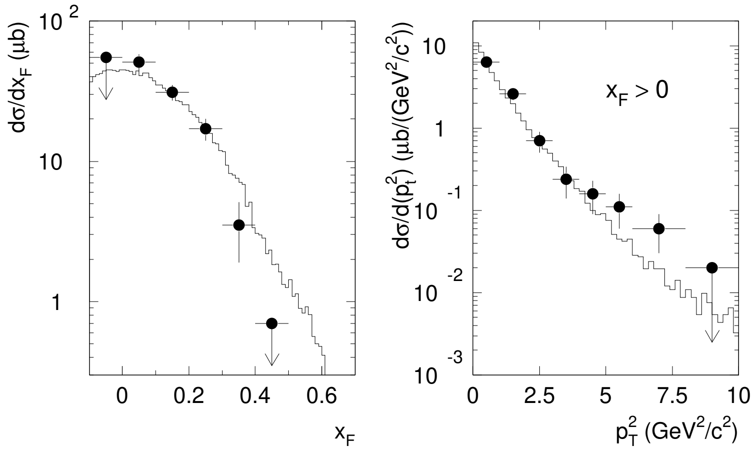

Figure 1.14: *x_F and p_T distributions for D mesons produced in p-p collisions at 250 GeV/c, compared with the scaled PYTHIA predictions[42]. See text for details.*

45 nucleon structure function set[28]. The solid line corresponds to the standard charm mass value $m_c = 1.5\ GeV/c^2$; the theoretical predictions for $m_c = 1.2\ GeV/c^2$ and $m_c = 1.8\ GeV/c^2$ are also shown. When theoretical uncertainties are taken into account, the hadro-production data are compatible with the value m_c=1.5 GeV/c^2.

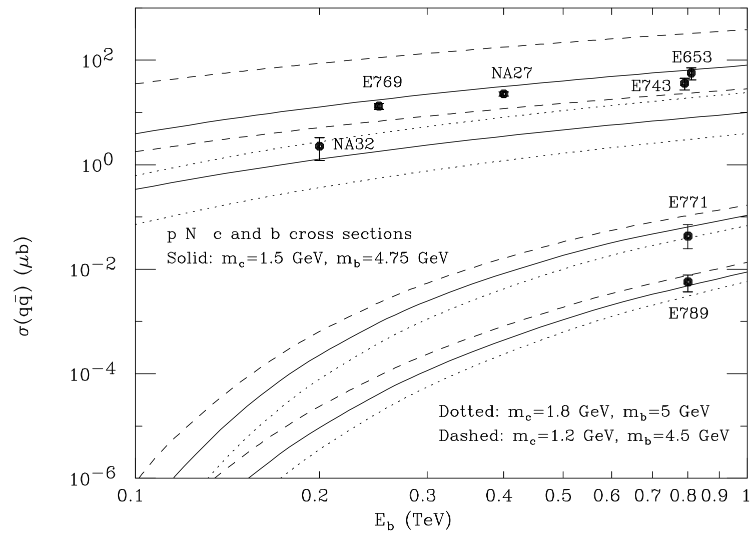

Figure 1.15: *Pair cross sections for c (and b) production in p-N collisions versus experimental results. The effect of changing the charm mass value is shown (top bands)[34]. See text for details.*

1.7 The dilepton mass spectrum

In Fig.1.16, where the 450 GeV/c pAg dimuon mass spectra measured by the NA50 experiment at CERN is shown, the different known contributing processes are indicated. In fig.1.17 the dielecron mass spectra measured by CERES in 450 GeV/c pBe and pAu collisions is also shown.

The dilepton differential mass spectrum can be subdivided in three different regions :

- The low mass region (LMR) for $M < 1.5\ GeV/c^2$.

  The low mass region can be still subdivided in two main regions : the low mass resonance region and the region below the ρ peak (M$\leq$750 MeV). The dilepton production in the region above the ρ peak is dominated by the leptonic decay of the ρ, ω ,ϕ vector mesons. Below the ρ peak dileptons are mainly produced in the Dalitz decay of hadrons, i.e.

$$\eta \longrightarrow l\bar{l}\gamma \tag{1.60}$$

$$\eta' \longrightarrow l\bar{l}\gamma \tag{1.61}$$

$$\omega \longrightarrow l\bar{l}\pi^0 \tag{1.62}$$

$$\pi^0 \longrightarrow l\bar{l}\gamma \tag{1.63}$$

- The intermediate mass region (IMR) for $1.5 < M < 2.5\ GeV/c^2$.

  In the IMR the following processes are known to contribute :

  - Dileptons from the DY process.
  - Dileptons from the semi-leptonic decay of charmed mesons and baryons.

- The high mass region (HMR) for $M > 2.5\ GeV/c^2$.

  The high mass region below the Υ consists of DY dileptons and dileptons produced in the decays of open-charm, J/ψ and ψ'; in particular, the region $4.5 < M < 8.0\ GeV/c^2$ consists of high mass DY dileptons only.

Another important contribution to the opposite-sign mass spectrum, both in the low and in the intermediate mass region, is the combinatorial background. The combinatorial background originates from the combination of leptons generated in the decays of K's and π's. Since the combinatorial background heavily contributes to the IMR spectra, its subtraction is one of the most important issues in the IMR data analysis. For instance, the background contribution in the IMR amounts to 85% in 450 GeV/c p-A and 200 A GeV/c S-U collisions and to 95% in 158 A GeV/c Pb-Pb central ones. A detailed description of the techniques used to compute the combinatorial background contribution to the opposite-sign mass spectrum can be found in chapter 5.

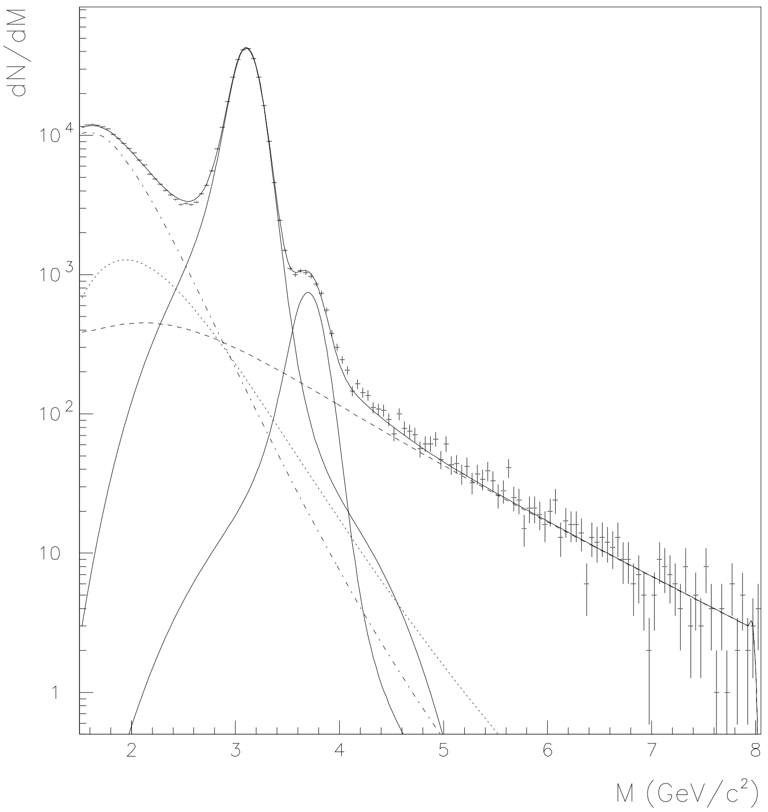

Figure 1.16: *Dimuon invariant mass spectrum of opposite-sign dimuons for the NA50 450 GeV/c pAg system. The processes contributing to the high and intermediate mass region are shown : the high mass J/ψ and ψ' resonances (full line), the DY muon pair (dashed line), the contribution from the semi-leptonic decay of charmed hadron pairs (dotted line) and the combinatorial background from the leptonic decay of kaons and pions (dash-dotted line).*

1.8 The dilepton production enhancement

The dilepton mass spectra, measured in proton induced collisions on nuclear targets, can be well described by a superposition of the known contributions listed in the previous section, as clearly shown in fig.1.17. On the other hand, an excess has been measured in the low and intermediate mass regions of the dilepton spectrum produced in nucleus-nuclues collisions at SPS energies. The measured dilepton yield exceeds the expected dilepton production as extrapolated from p-A interactions. Furthermore, the excess measured by CERES in the low mass region, suggests a stronger than linear dependence of the enhanced dilepton source on the collision centrality. Hard processes, like DY pair production and open charm hadro-production, are expected to linearly depend on the number of effective nucleon-nucleon collisions and the latter is predicted to linearly depend on the measured transverse energy

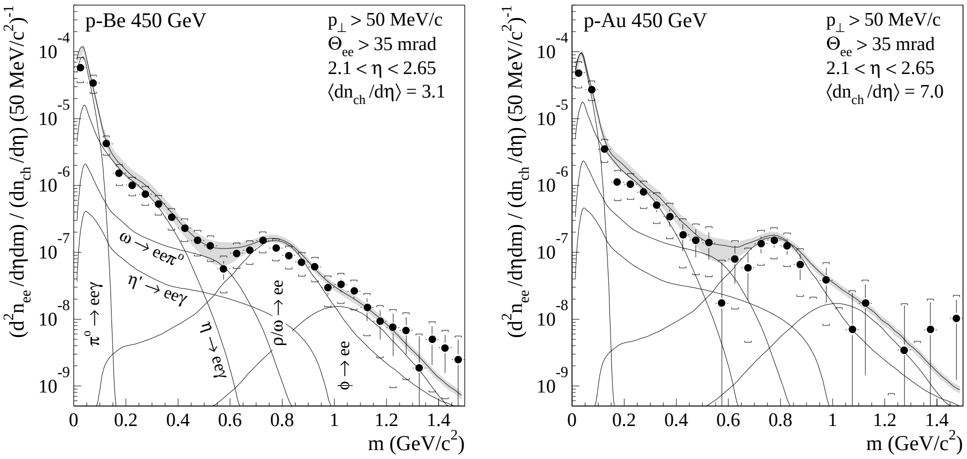

Figure 1.17: *Inclusive e^+e^- mass spectrum measured by CERES in 450 GeV/c p-Be and p-Au collisions in the low mass region. The thick line represents the summed yield of all the shown sources (dash-dotted lines).*

E_T[43]. The multiplicity of secondaries produced in a nucleus-nucleus collision is also proportional to E_T. On the other hand, the production of thermal dileptons from a thermalized QGP is expected to increase quadratically with the collision centrality[18]. In fact, when the production from the mixed quark-hadron phase is taken into account, an even more complicated dependence on the hadron multiplicity is predicted[44, 45]. Other processes could be responsible for an enhanced open charm production, as explained in chapter 7 (and references therein). A larger than linear dependence on the final hadron multiplicity and/or transverse energy E_T therefore clearly indicates the on-set of an alternative mechanism for lepton pair production.

In the following the results of the CERES, HELIOS/3 and NA38/NA50 experiments in the low and intermediate mass regions are discussed, along with the most promising theoretical interpretations of the found excess.

1.8.1 Experimental results

Evidence of an enhanced dilepton production in the LM and IM regions with respect to extrapolations from pA results, has been first observed in S induced collisions at 200 A GeV/c by the NA38 (S-U)[46, 47], CERES (S-Au)[48] and HELIOS/3 (S-W)[49] at the CERN SPS.

Preliminary results on Pb induced collisions were presented at the QM96 conference by NA50[50]; the measured $Data/(Expected - Sources)$ (or D/S) in the intermediate mass range for the (1992) 200 A GeV/c S-U and (1995) 158 A GeV/c Pb-Pb amounted to $D/S_{S-U,200AGEV/c}$=1.26±0.10 and $D/S_{Pb-Pb,158AGEV/c}$=2.03±0.09. In fig.1.18[50], the expected dimuon yield in 158 A GeV/c Pb-Pb collisions is compared with the measured dimuon mass spectrum. The two solid lines correspond to the expected charm production $\pm 1\sigma$. In fig.1.19[50] the excess measured by NA38/NA50 for the 200 A GeV/c S-U 1992 and 158 A GeV/c Pb-Pb 1995 data sets is plotted against the collision centrality. From the data presented at QM'96 it is difficult to conclude on the actual centrality dependence of the excess.

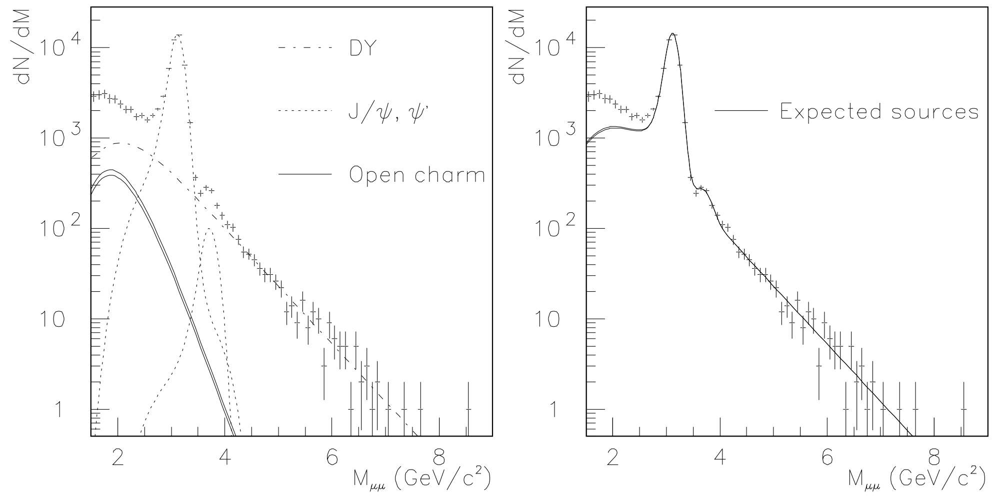

Figure 1.18: *Comparison of measured dimuon yield with expected sources in Pb-Pb collisions at 158 A GeV/c for the 1995 NA50 data set[50].*

CERES[51] at the same conference presented the results of the analysis of the 200 GeV/c S-Au low mass spectrum, where an excess is found for $M \geq 2m_\pi$. This threshold suggests that the observed excess could be due to the production of thermal dileptons in $\pi\pi$ (and $\pi\rho$) annihilations. The measured D/S ratio is 5.0±0.8(sta)±2(sys) for 0.2< M <1.5 GeV/c^2. CERES recently measured the excess in Pb-Au collisions at 158 A GeV/c, finding D/S=3.4 ± 0.4 ± 0.9 for 0.2< M <2.0 GeV/c^2. In fig.1.20 the CERES mass spectra for 158 A GeV/c Pb-Au is shown. The summed and individual contributions from hadronic decays is also shown and it clearly indicates that conventional sources alone can not reproduce the low mass spectra. In fig.1.21 the excess measured by CERES in 158 A GeV/c Pb-Au collisions is plotted as a function of the charged multiplicity[52]. Here again it is difficult to conclude about the actual centrality dependence of the excess, even if a quadratical dependence can not be excluded.

HELIOS/3 in its recent analysis of the 200 A GeV/c S-W data[53], finds an excess expanding from the low to the intermediate mass region, up to the J/ψ threshold.

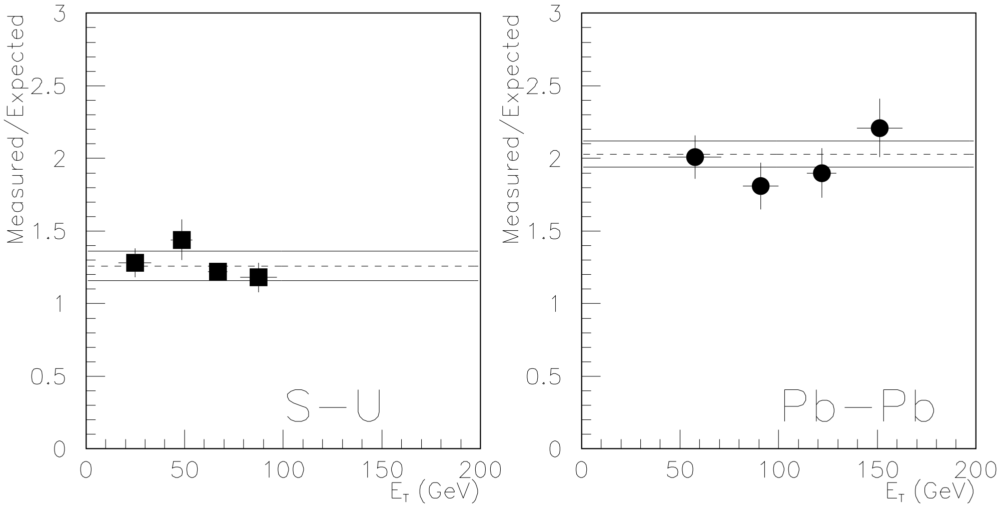

Figure 1.19: *Centrality dependence of the excess in the 1992 NA38 200 A GeV/c S-U and in the 1995 NA50 158 A GeV/c Pb-Pb data sets[50].*

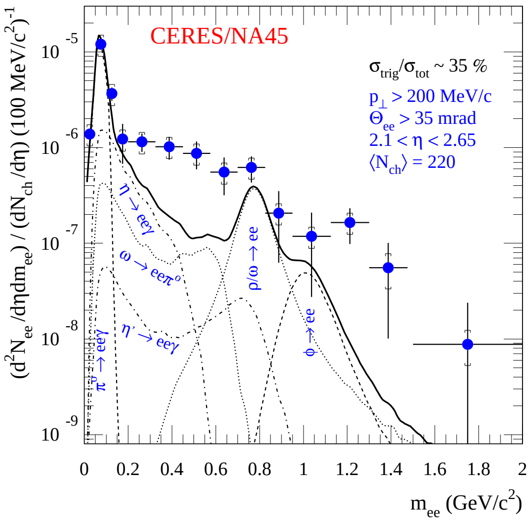

Figure 1.20: *Inclusive e^+e^- mass spectrum measured by CERES in 160 A GeV/c Pb-Au collisions normalised to the observed charged particle density. The individual and summed contributions from hadronic sources are also shown[52].*

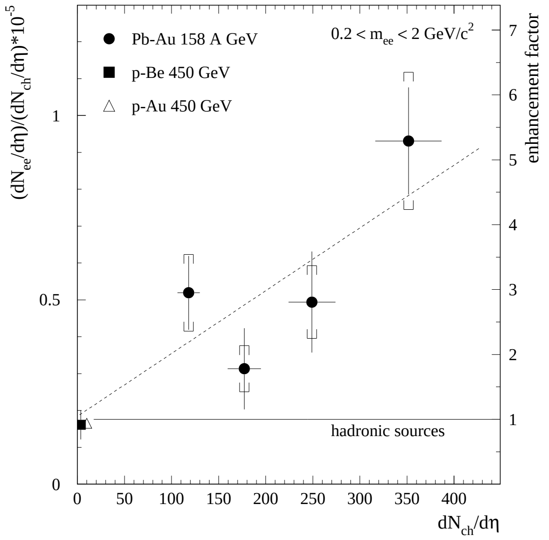

Figure 1.21: *Multiplicity dependence of the normalised pair yield for Pb-Au collisions as measured by the CERES Collaboration. Systematic and statistical uncertainties are shown separately. The dashed line represents a fit to the Pb-Au data assuming quadratical multiplicity dependence. The solid line represents the expectation from known hadronic sources. The normalised yield measured in proton-nucleus collisions is also shown[52].*

In the IMR, the measured D/S ratio is 5.91 ± 1.11 for 1.35< M <2.5 GeV/c^2 and 4.13 ± 1.24 for 1.6< M <2.5 GeV/c^2. In fig.1.22 the ratio D/S measured by HELIOS/3 in the IMR is plotted against the charged particle multiplicity[53]. Since the more peripheral bins are affected by a too little statistics, only the four charged multiplicity classes corresponding to the most central events have been analysed and are shown. It is therefore difficult to draw any definitive conclusion on the centrality dependence of the measured excess. In chapter 7 the results of the HELIOS/3 Collaboration will be discussed in some more detail in the attempt of drawing a comparison between their results and the results of the present work.

1.8.2 Comparison with theoretical models

When compared with the CERES experimental results, as shown in fig.1.23, the thermal dilepton contribution predicted in ref.[20] (see sec.1.5.4 of the present chapter) does not correctly reproduce the data for M≈500 MeV/c^2. A factor 10 enhancement in the total (QGP+HG) thermal dimuon yield is needed in order to describe the data. In fact, there is a general consensus in concluding that the additional production of thermal dimuons from a hadron gas alone can not account for the observed excess[16].

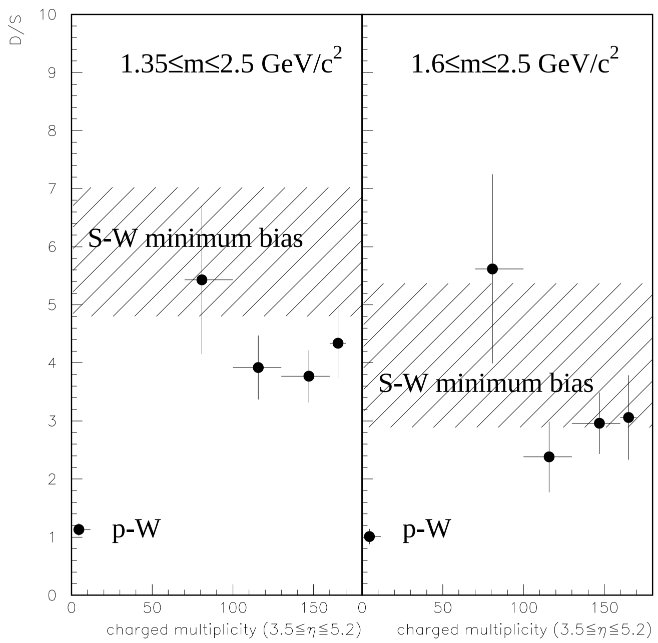

Figure 1.22: *Charged multiplicity dependence of the IMR dimuon excess as measured by the HELIOS/3 Collaboration[53]. The shaded areas correspond to Data/Sources*$=5.91 \pm 1.11$ *(left) and Data/Sources*$=4.13 \pm 1.24$ *(right).*

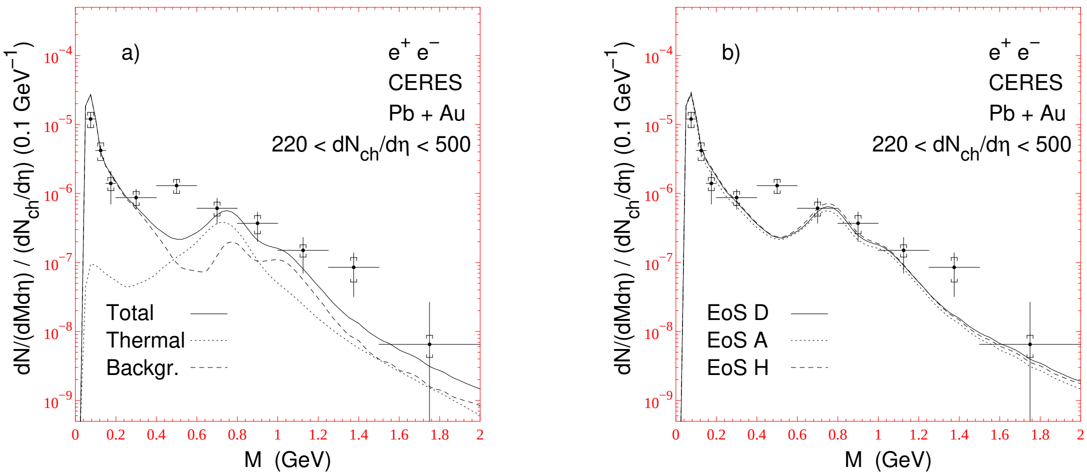

Figure 1.23: *Calculated electron pair spectrum compared to CERES data. (a) The emission from the fireball, background and the total spectra.(b) The total spectrum obtained using three different EoSs but always the same initial conditions. CERES kinematic cuts and experimental resolution have been taken into account[20].*

In fig.1.24 the low mass region data from CERES are compared to the prediction of the model described in ref.[54], where the thermal yield from a hadron gas is calculated including the ρ width broadening in the hot and dense medium with in-medium modifications of the ρ spectral function. In fig.1.25 the same model is compared to the low mass data of HELIOS/3.

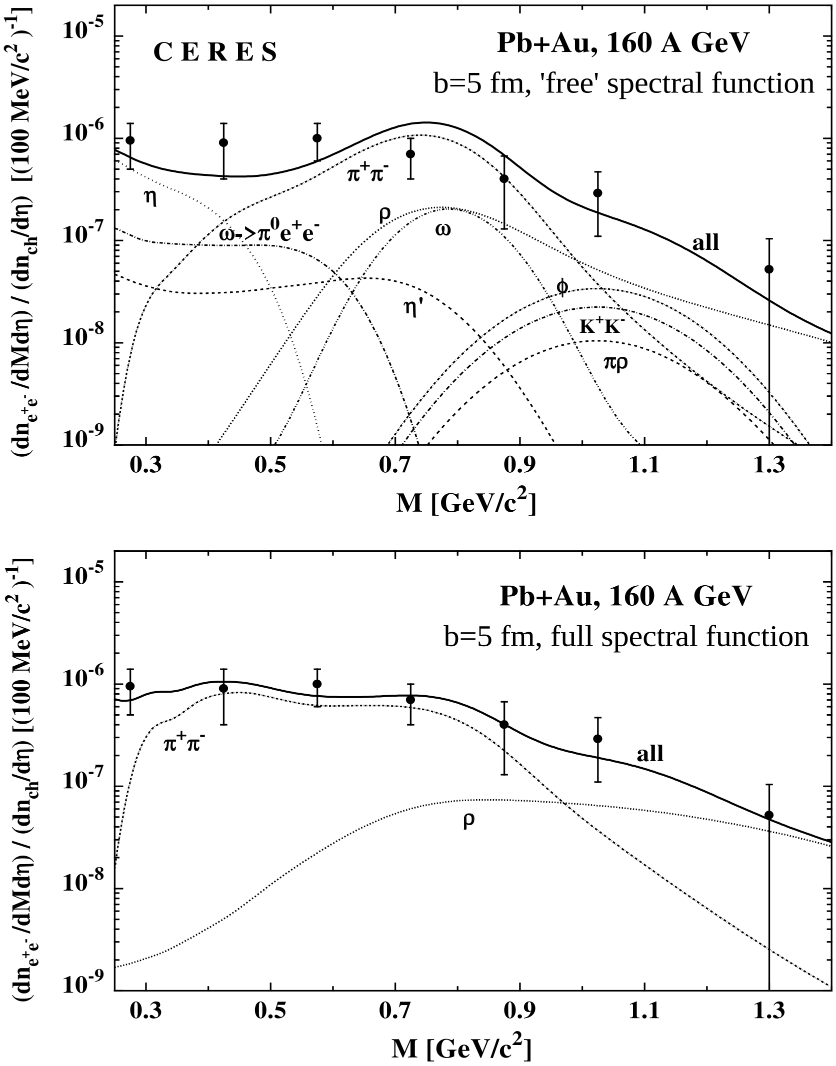

Figure 1.24: *Calculated dielectron invariant mass spectra for central 158 A GeV/c Pb-Au collisions compared to the CERES data[54], with (full) and without (free) in-medium modification of the ρ spectral function.*

In fig.1.26 the CERES and HELIOS/3 data are compared in the low mass region with the theoretical curves obtained in ref.[55] when the vector meson in-medium

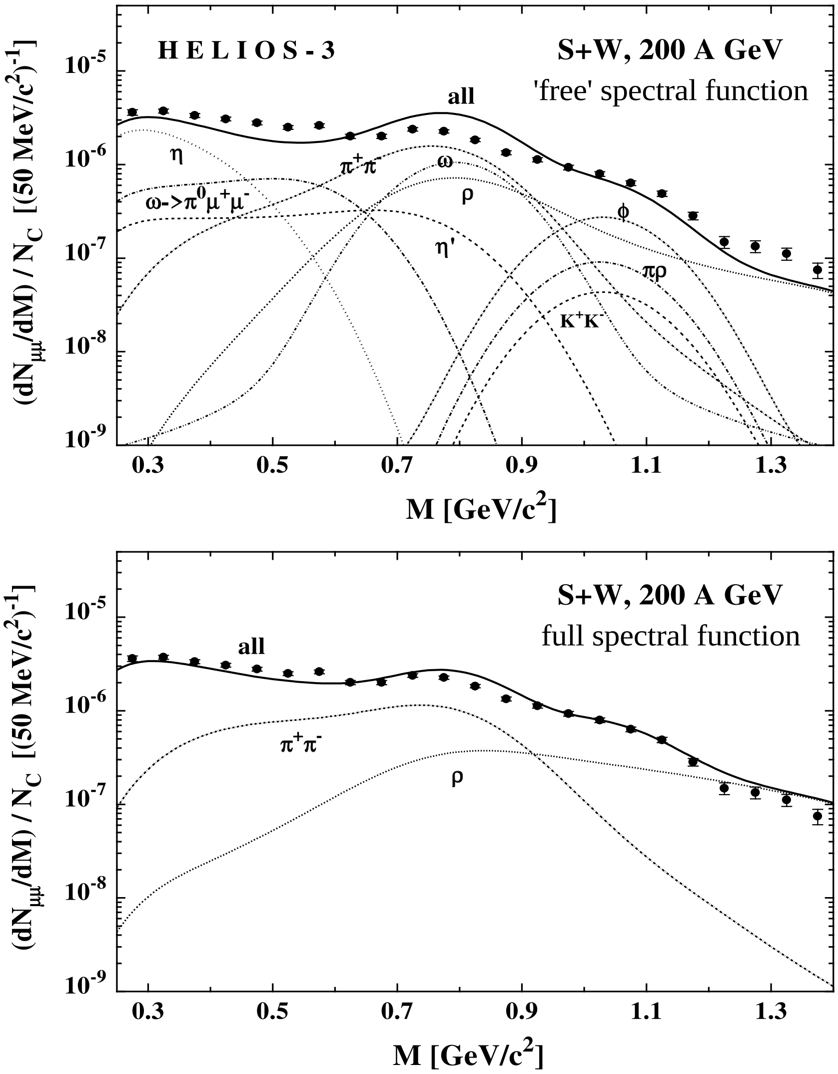

Figure 1.25: *Calculated dimuon invariant mass spectra for central 200 A GeV/c S-W collisions compared to the HELIOS/3 sets of data[54], with (full) and without (free) in-medium modification of the ρ spectral function.*

mass shift is taken into account.

In fig.1.27 the HELIOS/3 IMR data are compared with the model of ref.[19] (see sec.1.5.4 of the present chapter); the background contribution consists of dimuons from open-charm, DY and primary vector mesons, which is then added to the secondary contribution from thermal dimuons produced in a HG to give the final curve. The shape of the theoretical curve does not well reproduce the experimental mass spectrum in the range $1.5 < M < 2.5\ GeV/c^2$. The possible contributions from an enhanced charm production and/or secondary Drell-Yan pairs (see chapter 7) have not been included in the model. The inclusion of these mechanisms could perhaps lead to a better agreement between theoretical predictions and experimental data in the IMR for M> 1.5 GeV/c^2.

1.8.3 Previous knowledge and things to come

We have seen that for the low mass region some successful theories can well reproduce the observed excess in the dilepton spectrum. On the other hand, the excess measured in the intermediate mass region can originate from different sources (enhanced open charm production, secondary DY, thermal dileptons from a HG or QGP...), which actual role in the dimuon enhanced production is not yet clear. It is therefore necessary to assume $a-priori$ how to interpret the dilepton excess in the IMR and subsequently verify if a good description of all experimental data can be achieved within the chosen assumption.

In the present work the NA38/NA50 IMR excess is described as a simple superposition of dimuons from open-charm and DY, after combinatorial background subtraction. The 450 GeV/c p-A (NA50), 200 A GeV/c S-U (NA38) and 158 A GeV/c Pb-Pb (NA50, high statistics) sets of data are studied. The thermal dimuon contribution is not taken into account, because the theoretical description of such dimuon source is still affected by incertitudes.

It has been shown [42] that in order to describe the low mass region excess measured by CERES in S-Au collisions as originating from an enhanced open-charm production, the expected open-charm yield should be enhanced by a factor 150. Fig.1.28 from ref.[42] has been obtained in this hypothesis. Such a large enhancement factor is excluded by the results presented by the NA38/NA50 Collaboration at QM96 (see fig.1.18). Therefore, if the IMR excess originates from an enhanced open-charm production, this would clearly distinguish between the low and intermediate mass region excess.

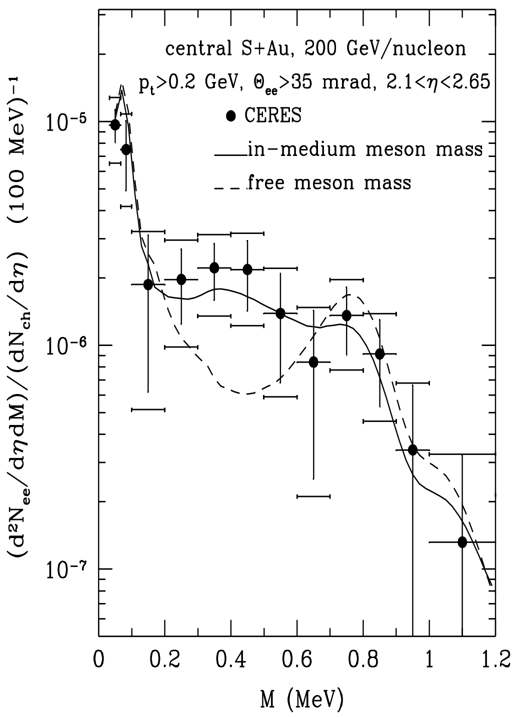

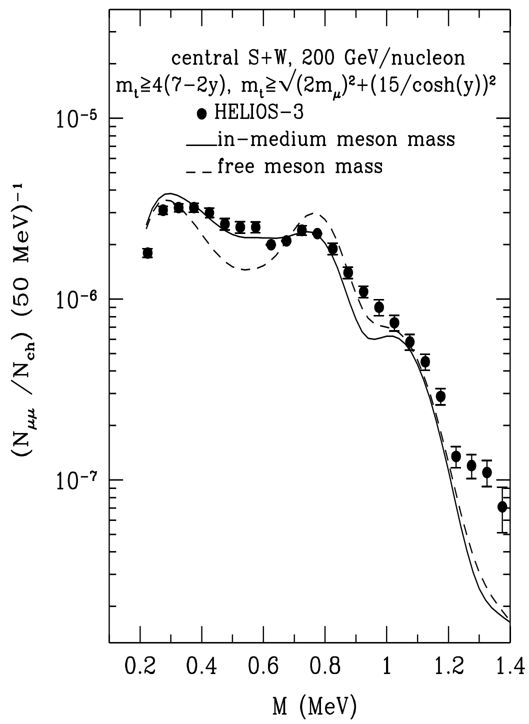

Figure 1.26: *CERES invariant mass spectra of dilepton from central 200 A GeV/c S-Au and HELIOS/3 invariant mass spectra of dilepton from central 200 A GeV/c S-W collisions compared with the theoretical curves obtained with (in-medium) and without (free) in-medium modification of the ρ mass shift[55].*

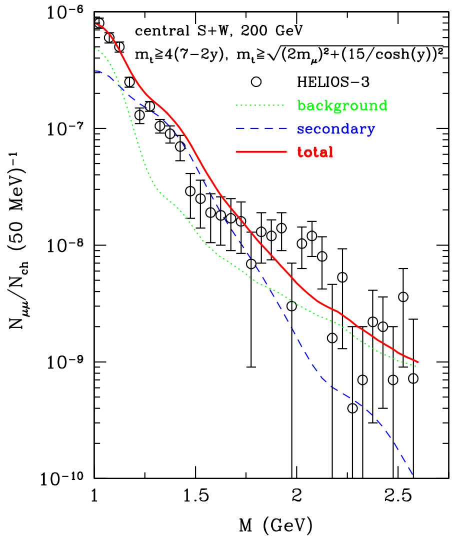

Figure 1.27: *Dimuon spectrum in central S-W collisions at 200 A GeV/c compared with calculations taking into account thermal dimuons from a hadron gas (indicated as secondary in the figure). The background contribution from open-charm, DY and primary vector mesons is added to the secondary contribution to give the total predicted yield.*

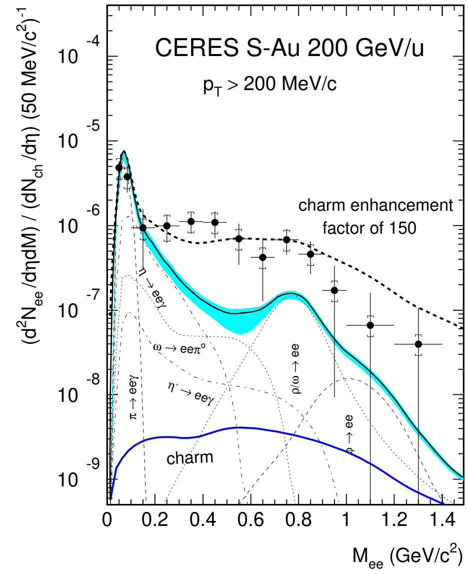

Figure 1.28: *Invariant mass spectrum of e^+e^- pairs measured by CERES in 200 A GeV/c collisions. The solid line gives the contribution expected from charm production in the standard scenario. The dashed line results from adding to the hadron decay background a charm contribution enhanced by a factor 150[42].*

Bibliography

[1] F.Karsh et al., Z.Phys.C-Particles and Fields 37 (1988)617

[2] Review of particle physics, The Eur.Phys.Journal, 1998.

[3] H.Satz, CERN-TH.7410/94

[4] E.Laermann, Nucl.Phys. A610 (1996) 1c-12c

[5] T.Matsui *et al.*, Phys. Lett. B 178 (1986) 416

[6] D.Kharzeev *et al.*, Z. Phys. C 74 (1997) 307-318

[7] Abreu M.C. *et al.* (NA50 collaboration), Phys.Lett. B410(1997)337

[8] J.Rafelski *et al.*, Phys. Rev. Lett. 48 (1982) 1066-1069

[9] J.Schaffner-Bielich, nucl-th/9711044 21 Nov 1997

[10] E.Anders et al., WA97 Collaboration, CERN-EP/98-64, 22 April 1998

[11] D.Jouan, for the NA38 Collaboration, at the Quark Matter '97 Conference, Japan (1997).

[12] A.Shor, Phys.Lett. B215 (1988)375.

[13] A.Shor, Phys.Lett. B233 (1989)231.

[14] P.Levai et al., Phys.Rev. C 56-5(1997)2707-2717

[15] P.V.Ruuskanen, Nuclear Physics A525 (1991) 255c-268c.

[16] R.Baier *et al.*, Invited talk at the 28th International Conference in High Energy Physics, Warszawa (1996).

[17] L.H.Xia et al., Phys.Rev. C 41, no.2 (1990) 572

[18] R.C.Hwa et al.,Phys.Rev D 32,no.5 (1985) 1109

[19] G.Q.Li et al., Preprint nucl-th/9807005 (1998)

[20] P.Huovinen *et al.*, Preprint nucl-th/980707

[21] B.Friman, Nucl. Phys. A610 (1996) 358c-372c

[22] T.Hatsuda *et al.*, Nucl. Phys. A590 (1995) 545c-548c

[23] Ito et al. E288 Collaboration, Phys.Rev. D23 (1991) 604

[24] A.Baldit et al., Phys.Lett., B332 (1994)244-250

[25] A.D.Martin et al., hep-ph/9409257

[26] A.D.Martin et al., Phys.Rev. D 51(1995)4856

[27] M.Gluck et al., Z.Phys. C53 (1992) 127

[28] PDFLIB 7.09, Users's Manual, CERN/PPE (1997)

[29] K.J.Eskola, Preprint hep-ph/9807297, 1998

[30] J.J.Aubert et al., the EMC Collaboration, Phys.Lett. 123B, no.3,4 (1983) 275

[31] A.Bodek et al., Phys.Rev.D 23,no.5 (1981) 1070

[32] C.Lourenço, Ph.D. thesis, Universidade tecnica de Lisboa, 1995

[33] N.Armesto, Preprint hep-ph/9609296, 1996

[34] S.Frixione et al., CERN-TH/97-16, hep-ph/9702287

[35] S.J. Brodsky et al., Nucl.Phys. B360 (1991)67-96

[36] S.J. Brodsky et al., Nucl.Phys. B383 (1992)643-684

[37] S.J. Brodsky et al., Nucl.Phys. B 438 (1995)261-277

[38] H.Nowak, Fortschritte der Physik, 39, no.5,6 (1991) 347

[39] M.J.Leitch et al. (E789 Collaboration), Phys.Rev.D51(1995)4756

[40] G.A. Alves et al. (E769 Collaboration), Phys.Rev.Lett.70 (1993)722.

[41] M.Adamovich et al., Nucl.Phys. B 495 (1997)3-34

[42] P.Braun-Munzinger *et al.*, subm. Z.Phys. C (1997)

[43] J.Ftacnik et al.,Phys. Lett. B196, no.3, 1987

[44] M.I.Gorentstein et al., Z.Phys.C-Particles and Fields 37 (1988)611; M.I.Gorentstein et al., Phys.Lett. 192,np1,2 (1987)198

[45] B.Kampfer et al., Z.Phys.C-Particles and Fields 45 (1990) 491

[46] C.Lourenco, for the NA38 Collaboration at the Quark Matter '93 Conference, Borlange, Sweden (1993).

[47] C.Lourenco, for the NA38 Collaboration, Proc.of the 5th Conference on Intersections between Particle and Nuclear Physics, St.Petersburg, FL(1994)

[48] P.Wurm, for the NA45/CERES Collaboration at the Quark Matter '95 Conference, Monterey, California, USA (1995)

[49] M.Masera, for the HELIOS/3 Collaboration at the Quark Matter '95 Conference, Monterey, California, USA (1995)

[50] E.Scomparin, for the NA50 Collaboration, at the Quark Matter '96 Conference, Heidelberg, Germany (1996),Nucl. Phys., A : 610(1996) (331c-341c).

[51] Th.Ullrich, for the NA45/CERES Collaboration, at the Quark Matter '96 Conference, Heidelberg, Germany (1996).

[52] G.Agakichiev *et al.*, nucl-ex/9712008 (1997), sub. Phys. Lett. B, 422(1998)405 1/4

[53] A.L.S.Angelis *et al.*, the HELIOS/3 Collaboration, CERN-EP/98-82 and to be submitted to Zeit.fur.Physik.

[54] W.Cassing *et al.*, Preprint nucl-th/9708020, Subm. to Phys. Rev., C. (13 p) (1997)

[55] G.Q.Li *et al.*, Nucl.Phys. A611, 539 (1996)